University of Natural Resources
and Life Sciences, Vienna

Master Thesis

Rolling circle amplification for plasmonic biosensors

Submitted in partial fulfilment of the requirements
for the academic degree of
Diplomingenieurin (Dipl.-Ing.^{in}) or
Master of Science (MSc) in Biotechnology

Submitted by
Bernadette LECHNER, BSc
01441351

November 2020

AIT – Austrian Institute of Technology
CEST – Competence Centre for electrochemical Surface Technology
BOKU – University of Natural Resources and Life Sciences

Supervised by: Dr. Jakub Dostálek – Biosensor Technologies (AIT)
Prof. Dr. Erik Reimhult - Department of Nanobiotechnology (BOKU)

University of Natural Resources
and Life Sciences, Vienna

Affidavits

I hereby declare that I am the sole author of this work. No assistance other than that which is permitted has been used. Ideas and quotes taken directly or indirectly from other sources are identified as such. This written work has not yet been submitted in any part.

Eidesstattliche Erklärungen

Ich erkläre eidesstattlich, dass ich die Arbeit selbständig angefertigt habe. Es wurden keine anderen als die angegebenen Hilfsmittel benutzt. Die aus fremden Quellen direkt oder indirekt übernommenen Formulierungen und Gedanken sind als solche kenntlich gemacht. Diese schriftliche Arbeit wurde noch an keiner Stelle vorgelegt.

Bernadette Lechner, November 2020

Acknowledgements

First of all, I want to express my deepest gratitude and appreciation to Dr. Jakub Dostálek for giving me the opportunity to work in his group. His consistent support and insightful feedback helped me to sharpen my thinking and look at things from different perspectives.

I especially pay my sincere regards to Dipl.-Ing.in Simone Hageneder, for her invaluable assistance and patience in instructing me. She passionately shared her expertise and always encouraged me, whenever I ran into troubles.

I acknowledge Prof. Dr. Erik Reimhult for his kind offer to supervise and review my thesis.

Additionally, I wish to thank all people from the Biosensor Technologies group at the AIT. They received me with open arms and contributed with professional advice, while still giving me the freedom, to do things in my own way.

I also want to thank my dearest friends Anna, Jasmin and Lisa for all the late hours of studying and delightful distractions throughout my studies. I am extremely thankful for every shared moment with you guys.

Last but not least, I am extremely grateful for the great love of my parents and my loved one, Isak. Without their unconditional support and granted trust, it would have not been possible to complete this thesis and achieve my goals.

Abstract

The detection of specific nucleic acids holds great potential to investigate the presence of various genes which are associated with genetic and infectious diseases. Particularly for the diagnosis of infectious diseases, there is a great need for medical devices to obtain fast, accurate and reliable information of such sequence-specific nucleic acids.

This thesis deals with the detection of antibiotic resistance genes, by employing a ligation-based padlock probe concept on an optical biosensor. Circularized padlock probes were enzymatically amplified by rolling-circle amplification (RCA) at room temperature. The combination of surface plasmon resonance (SPR) with surface-plasmon fluorescence spectroscopy (SPFS) is used to detect minute amounts of the fluorophore labeled amplification products.

As a first step, the assay concept, including padlock circularization and subsequent isothermal nucleic acid amplification through RCA is demonstrated in the liquid phase. The generation of RCA product was visualized by standard agarose gel electrophoresis.

Secondly, the assay was implemented on a plasmonic biosensor. SPR and SPFS detection principle allowed to monitor and confirm the surface-initiated growth of single-stranded DNA strands. The reaction was investigated towards the specificity of fluorophore labeling of the RCA product as well as hybridization of the padlock to the sensor surface.

The time-dependent growth of densely packed DNA brushes was monitored in-situ by optical waveguide spectroscopy (OWS). The length of the surface-bound DNA and the extension rate of ϕ29-DNA polymerase was determined.

Additionally, a concept to control the growth of the long DNA strands to the sensor surface is shown and a possible route for the rapid detection of antibiotic resistance genes in a multiplexed format is proposed.

Zusammenfassung

Der Nachweis spezifischer Nukleinsäuren birgt großes Potenzial zur Detektion verschiedener Gene, die mit genetischen und Infektionskrankheiten assoziiert sind. Insbesondere für die Diagnose von Infektionskrankheiten sind neue Teststrategien erforderlich, um schnelle und zuverlässige Informationen über die Infektion mit resistenten Bakterien zu erhalten.

Diese Arbeit befasst sich mit dem Nachweis von Antibiotikaresistenzgenen durch die Verwendung von zirkularisierten Padlockproben auf einem optischen Biosensor. Die Padlockproben wurden enzymatisch bei Raumtemperatur durch Rolling-Circle-Amplifikation (RCA) amplifiziert. Die Kombination von Oberflächenplasmonenresonanz (SPR) mit Plasmonenfeld-verstärkter Fluoreszenzspektroskopie (SPFS) wird verwendet, um winzige Mengen von den mit Fluorophoren markierten Amplifikationsprodukte nachzuweisen.

In einem ersten Schritt wird das Assay-Konzept einschließlich der Padlockzirkularisierung und der anschließenden DNA-Amplifikation mittels RCA in der flüssigen Phase demonstriert. Die Erzeugung des RCA-Produkts wurde durch Agarose-Gelelektrophorese sichtbar gemacht.

Zweitens wurde der Assay auf einem plasmonischen Biosensor durchgeführt. Das SPR- und SPFS-Nachweisprinzip ermöglichte die Überwachung und Bestätigung des Wachstums einzelsträngiger DNA-Stränge an der Sensoroberfläche. Die Reaktion wurde auf die Spezifität der Fluorophormarkierung des RCA-Produkts, sowie der Hybridisierung der Padlockproben an die Sensoroberfläche untersucht.

Das zeitabhängige Wachstum dicht gepackter DNA-Bürsten wurde in situ durch optische Wellenleiterspektroskopie (OWS) überwacht. Die Länge der oberflächengebundenen DNA-Stränge und die Verlängerungsrate der ϕ29-DNA-Polymerase wurden bestimmt.

Zusätzlich wird ein Konzept zur Steuerung des Wachstums der langen DNA-Stränge zur Sensoroberfläche gezeigt und ein möglicher Weg zum schnellen Nachweis von Antibiotikaresistenzgenen in einem Multiplexformat vorgeschlagen.

Contents

List of Abbreviations

AST	Antimicrobial Susceptibility Testing
ATR	Attenuated Total Reflection
AuNP	Gold Nanoparticle
BRE	Biological Recognition Element
DNA	Deoxyribonucleic Acid
LOD	Limit of Detection
MIC	Minimal Inhibitory Concentrations
OEG	Oligoethylene glycol
PCR	Polymerase Chain Reaction
PEF	Plasmon-enhanced Fluorescence
PLP	Padlock Probe
PSP	Propagating Surface Plasmon
RCA	Rolling Circle Amplification
RIU	Refractive Index Unit
RNA	Ribonucleic Acid
SAM	Self-assembled Monolayer
SPFS	Surface Plasmon Fluorescence Spectroscopy
SPR	Surface Plasmon Resonance

1. Antibiotic resistance

According to the world health organization (WHO), antimicrobial resistance (AMR) is an increasing threat to global health. It can affect everyone, it occurs naturally and misuse of antibiotics accelerates the process of the evolvement of so-called superbugs, pathogens resistant to several different antimicrobial agents.[1,2] 700,000 deaths are currently ascribed to antimicrobial resistance. It is estimated that this number can rise to 10 million by 2050.[3,4]

Antibiotic resistance (AR) is the ability of bacteria to withstand the effects of antibiotics and making them ineffective.[5] The first antibiotic was penicillin, discovered by Andreas Fleming in 1929.[6] Even before penicillin found its way into medical treatment, its inactivation through penicillinases has been described.[7] Penicillinases are a specific type of *β*-lactamases, enzymes encoded and expressed by bacteria providing them antibiotic resistance. This feature can be intrinsic in certain bacterial strains but also be acquired through horizontal gene transfer and mutations in chromosomal genes.[8,9] *β*-lactams (e.g. cephalosporins, monobactams and carbapenems) are the most used antibiotics in the medical treatment of infectious diseases.[10,11] Especially carbapenem resistance, acquired by bacteria through encoding OXA *β*-lactamases, is considered as a major threat towards multi-drug resistant species. The high mutation rate of this sequence, in particular the *bla*$_{OXA}$-type, gave rise to several variants and has already been detected worldwide.[12–15]

Antibiotic resistance can be determined in several ways and include phenotypic as well as genotypic characterization. The first detection method relies on *in vitro* testing and the determination of so-called minimal inhibitory concentrations (MIC) or inhibition zones in microbiological laboratories.[16] This standardized method, also known as antimicrobial susceptibility testing (AST) allows to identify a pathogen's resistance by exposing it to different antibiotics and found its daily application in routine diagnostics.[17]

In the past decade, several DNA-based assays have been developed to detect antimicrobial resistance at the genetic level. Microarrays, nucleic acid amplification techniques and whole-genome sequencing (WGS) in automated instruments promise an

increased specificity, sensitivity and speed and offer the detection of multiple known resistance genes in one test. Besides that, matrix-assisted laser desorption ionization-time of flight mass spectrometry (MALDI-TOF MS) can provide substantial information about protein expression and product degradation in bacteria.[18,19] An overview of current and emerging techniques is given in several reviews.[20–22]

1.1. Phenotypic antibiotic susceptibility testing

Traditionally three methods are used in AST, including the disk diffusion, broth dilution and agar dilution method.[17] Figure 1 shows the most common tests to perform phenotypic AST. In agar disk diffusion methods, paper disks containing a defined concentration of antimicrobial agents are placed on precultured agar plates. After incubation, the diameter of the growth inhibition zones is determined. This method allows simultaneous testing of several antimicrobial agents, but only gives qualitative results.

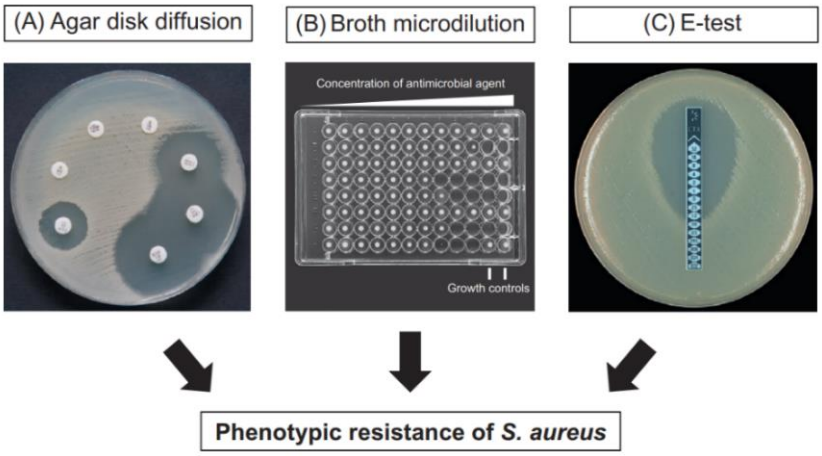

Figure 1: Antibiotic susceptibility testing for phenotypic characterization of pathogen's resistance (reprinted from [17]).

Contrary to that, broth microdilution methods also provide an easy and quantitative determination of antibiotic susceptibility. Commercially available microtiter plates, allow standardized testing in automated instruments. The wells already contain dilution series of freeze-dried antimicrobial agents and are inoculated with the pathogen containing medium. Those automated systems employ fluorescence and colorimetric techniques as well as the attenuation of light to follow bacterial growth. Based on this

detection principle systems from VITEK®, BD Phoenix™, Sensititre™ and Micro-scan walk away® found its way into clinical microbiology.[23]

Furthermore, E-tests give quantitative results and MIC values can be determined by placing a plastic strip, containing a concentration gradient of an antimicrobial agent, onto an agar plate with a standardized inoculum.[17] However, all those methods still require a pure culture of bacteria. Purification and strain identification take 24 hours up to several days. Additional AST and reporting of results take another 1-3 days. This delay in time leads to the administration of broad-spectrum antibiotics and often leads to ineffective treatment. Extended hospital stays, higher medical costs and increased mortality are the consequences.[24]

1.2. Genotypic characterization of antibiotic resistance genes

The detection of antibiotic resistance genes towards a rapid detection of specific sequences promises advances in genetic screening and pathogen detection, eliminating the tedious cultivation of bacteria and its purification.[25] Polymerase chain reaction (PCR) has become one of the most efficient molecular tools to amplify small amounts of DNA sample exponentially (see Figure 2).[26] Denaturation leads to the single-strand formation of the target gene containing DNA (dsDNA). Specially designed primers (blue, red) bind to specific regions (annealing) of the target gene before the enzymatic extension is conducted by polymerases (e.g. Taq Polymerase). This thermal cycling is usually repeated 20-40 times to obtain sufficient genetic material.

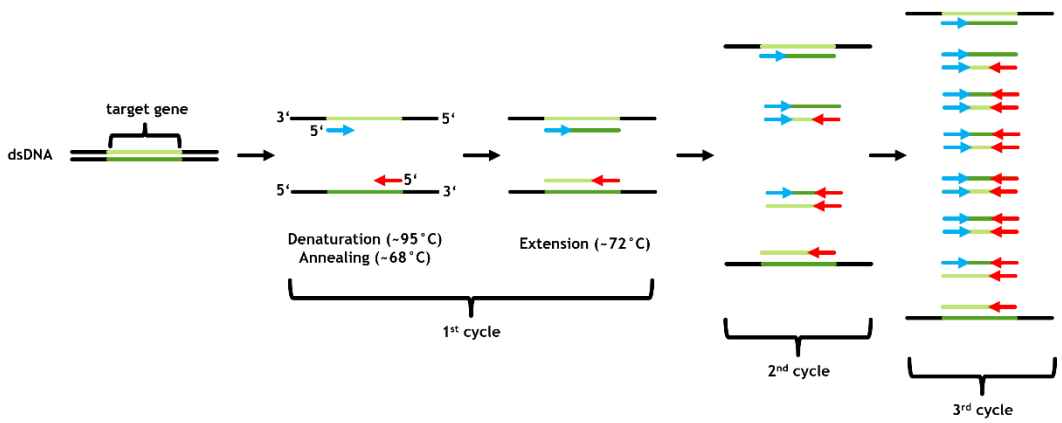

Figure 2: Schematic of target gene amplification in a PCR thermocycler (based on figure in [27]).

Doyle et al. showed multiplex PCR detection of encoded carbapenemase genes., detecting five *β*-lactamase sequences (*bla*$_{KPC}$, *bla*$_{NDM}$, *bla*$_{OXA-48-like,}$ *bla*$_{VIM}$, and *bla*$_{IMP}$) through the addition of multiple primer sets showing 100% sensitivity and specificity.[28] However, to get detectable signals, usually a high copy-number of target gene has to be present, making DNA extraction and pre-amplification steps necessary. Moreover, PCR products have to be visualized via gel electrophoresis.

Quantitative PCR (qPCR) enables real-time monitoring of the amplification process. Quantification is mostly achieved by introducing fluorescent dyes like SYBR® Green[29], which intercalate double-stranded DNA (dsDNA). Also, TaqMan probes[30] have been used for the detection of an amplification product. They are designed to hybridize to their complementary sequence before Taq polymerase cleaves off the fluorophores and the emitted fluorescence light can be detected.

Also, the usage of molecular beacons and fluorescence resonance energy transfer (FRET) hybridization probes found application in PCR product quantification.[31,32] Nevertheless current PCR techniques are limited to detect only four to six target genes in one sample[33], making the detection of several resistance genes expensive and time-consuming.[34,35]

1.2.1. Microarray technology

Since the first oligonucleotide immobilization on a solid support in 1965, the interest into its application increased tremendously.[36] Grunstein and Hogness showed the possibility to screen 1000's of colonies by hybridizing radiolabelled DNA probes with their complementary sequences.[37] Further development in the immobilization strategies of DNA and peptides and the implementation of fluorescence detection gave rise to the modern DNA microarray.[38] Especially fluorescence labeling improved the accuracy and speed of hybridization events. In comparison to radioactive and chemiluminescent labeling, it is more sensitive, less expensive and simpler. Moreover using different dyes allows multiplexing and the detection of different hybridization reactions on the same array.[39,40]

Several research groups published the fabrication of DNA microarrays detecting antibiotic resistance genes or 16S rRNA genes, phylogenetic markers to identify bacteria at the species level.[41–44] Commercialized microarray products have been described and compared elsewhere.[45–47] Wolff et al. showed the possibility to fabricate low-cost microarrays, elongating immobilized DNA strands through terminal deoxynucleotidyl transferase (TdT) and biotin-conjugated nucleotides.[48] Labelling with Alexa Fluor 647 conjugated streptavidin reduced the costs by about tenfold.

Nonetheless, cross-hybridization (non-specific hybridization) of dissolved DNA to immobilized DNA targets still leads to limitations of microarray panels.[49] Hence the combination with enzymatic reactions has shown to increase specificity and sensitivity.[50,51] Ericsson et al. employed on-chip ligation to improve specificity in connection with subsequent rolling circle amplification (RCA) to multiply the signal intensity of a single-binding event.[52]

1.2.2. Rolling circle amplification

Rolling circle replication (RCR) is an enzymatic process to replicate DNA and RNA unidirectional.[53] This mechanism of synthesizing multiple copies of a circular DNA or RNA template is commonly used by bacteriophages and viruses, enabling them to produce several hundreds of copies of their plasmids and genomes.[54,55] The most relevant feature of RCR is that the newly synthesized strand remains covalently attached to the parental strand, which only gets elongated on its 3'-end.

RCA uses this mechanism, taking the most advantage of the fact that nucleic acids get amplified at isothermal reaction conditions.[56] Therefore, this type of amplification has emerged as a robust alternative to conventional PCR. It neither requires thermocycling nor a specific set of primers.[57] This simple and efficient process utilizes DNA and RNA polymerases to generate long ssDNA strands. Figure 3 shows the hybridization of a primer sequence to its complementary sequence on the circular probe. The primer gets elongated through a polymerase which catalyses the sequential incorporation of nucleotides at the primers free 3'-OH group. Through this process a

long single-stranded DNA strand is generated, which contains a set of repetitive sequences complementary to the circular template.

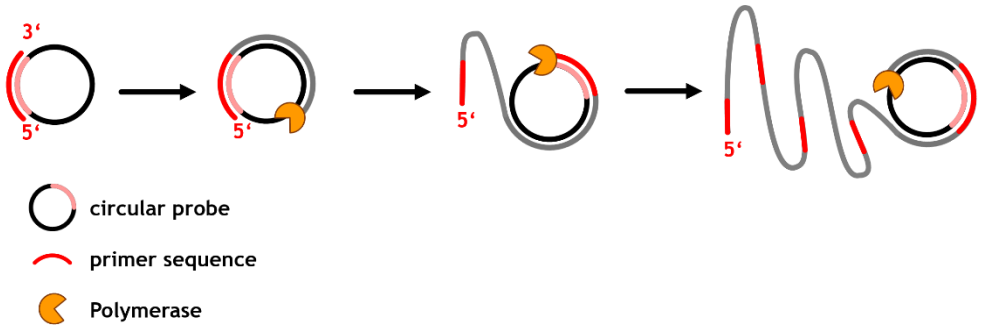

Figure 3: Principle of rolling circle amplification RCA (based on figure in [58]).

Due to its excellent strand displacement and highly processive activity on circular DNA templates,[59] Phi29 bacteriophage (Φ29) DNA polymerase makes RCA a promising tool for the ultrasensitive and ultrafast detection of DNA. Also functional acids, such as aptamers and DNAzymes can be amplified.[60] Several reviews discuss the progress of RCA and its applications in molecular diagnostics and material sciences.[61,62] It should be noted, that nucleic acids can also be amplified through loop-mediated isothermal amplification (LAMP), helicase-dependent amplification (HDA), recombinase polymerase amplification (RPA) and hybridization chain reaction (HCR).[57] An overview of those molecular amplification methods for point of care (POC) diagnostics was given by Lau and Botella.[58]

1.2.3. Padlock probes as circular templates

When it comes to the detection of single nucleotide polymorphisms (SNP) or specific gene segments, designed padlock probes (PLPs) can enhance the specificity and of RCA-based assays, simultaneously enabling multiplex detection.[63,64] PLPs (see Figure 4) are synthetic linear single-stranded oligonucleotides, composed of two target-complementary sequences (dark green) connected by a linker, which may contain a unique detection sequence (red).[65]

Upon binding of the 3' and 5' terminal regions to a target gene, the two ends (also called ligation nicks) can be joined by a DNA ligase. This enzyme-mediated reaction is highly specific. Thus, the PLP only gets circularized if the nucleotides at the junction are hybridized to the complementary target sequence.

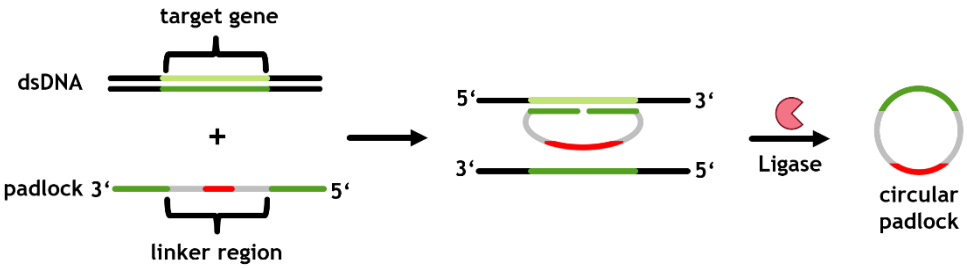

Figure 4: Principle of padlock probe assay (based on figure in [58]).

In the last years, ligase-mediated padlock circularization in combination with subsequent isothermal amplification via RCA and its capability to detect multiple resistance genes of pathogens was thoroughly investigated.[66] The generated RCA products can be sensitively detected by tethering complementary oligonucleotides to functional moieties. For that, mostly modified nanoparticles[67], electrochemical tags[68], antibodies and fluorescent dyes are used.[69,70] The implementation of this technique is further discussed in chapter 3.

2. Biosensors

A biosensor is an analytical device converting a biological or chemical reaction into a measurable electrical or optical signal.[71] The sensor consists of two main components and uses a biological recognition element (BRE) immobilized on the sensor surface which selectively or specifically interacts with the target analyte. The signal is transmitted to the transducer element that probes this interaction and converts it to a signal.[72]

Figure 5 schematically shows the principle of an optical biosensor, where different biological and chemical analytes like heavy metals, toxins and viruses are recognized and bound by antibodies, enzymes and aptamers leading to a change in the optical signal of the transducer, followed by signal processing.[73]

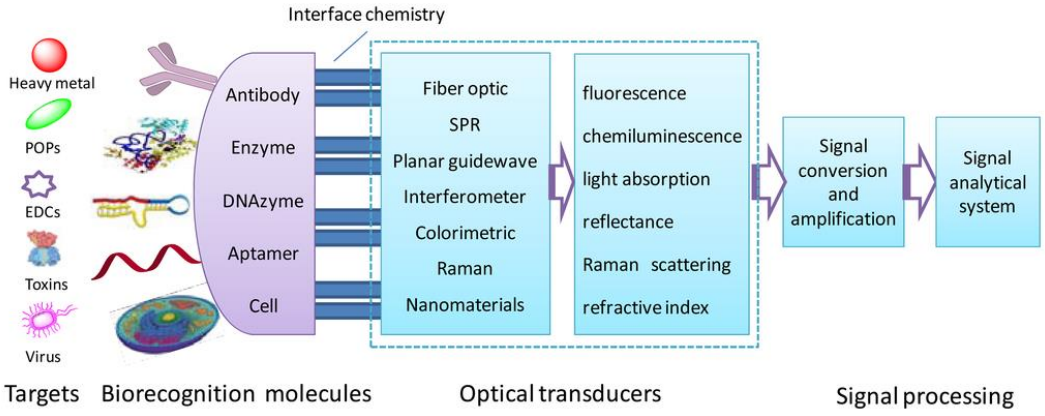

Figure 5: Schematic showing the main components of an optical biosensor (reprinted from [73]).

Biosensors offer a great possibility to monitor biological processes in a fast and reliable way, which is of utmost importance for disease detection and drug discovery in medical diagnostics as well as in food analysis and environmental monitoring.[71,74] The performance of biosensors is described by its sensitivity and specificity towards a biochemical reaction. Therefore the selection of a suitable transducer, a specific BRE and its immobilization on the transducer surface is crucial to detect target analytes in complex mixtures.[75]

2.1. Plasmonic biosensors

Biosensors based on surface plasmon resonance (SPR) are optical biosensors enabling a direct, label-free and real-time detection of chemical and biological components in a quantitative manner.[76,77]

Since the first sensor demonstrated the ability to study processes on thin metal surfaces in the early 1980s, the interest in developing SPR biosensors increased steadily.[78] Plasmonic biosensors use the excited surface plasmon field to probe changes of the refractive index at the interface of a thin metal surface and a dielectric medium in a highly sensitive manner.[79]

Figure 6 shows an example of the sensor surface with a BRE, shown in green. Upon binding of the target analyte, indicated as red triangles, the refractive index in the vicinity of the metal surface changes, which alters the coupling conditions of surface plasmons that probe the interface and thus can be converted to an optical signal.[80–82]

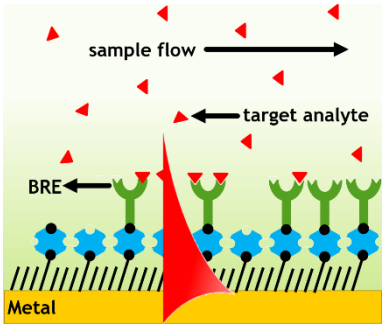

Figure 6: Scheme of a plasmonic biosensor showing the binding of a target analyte to the biofunctionalized sensor surface which is probed by a surface plasmon field at a metal-dielectric interface.

SPR biosensors enable the direct and sensitive detection of biomolecular interactions of target analytes to the monolayer of anchored BRE down to the pM range.[83] However, the limit of detection (LOD) strongly depends on the molecular weight of the target analyte. In case of low molecular weight analytes (M_W <1000 Da), the change in refractive index is often not measurable for most state of the art SPR instruments.[84] Therefore plasmon-enhanced spectroscopy methods and signal amplification strategies enabled the detection of small ligands at even lower concentrations leading to an improved LOD.[85] Those include surface-enhanced Raman

spectroscopy (SERS), surface-enhanced infrared absorption spectroscopy (SEIRAS) and surface plasmon fluorescence spectroscopy (SPFS).[86,87] The latter will be further described in chapter 2.3.

2.2. Surface plasmon resonance

Propagating surface plasmons (PSPs) are defined as optical waves travelling at the metal-dielectric interface, originating from collective oscillations of electron plasma in metals.[88] These oscillations can build up an electromagnetic field, which penetrates the two adjacent media perpendicular to the interface while the majority of the field intensity is confined in the dielectric. Many parameters influence coupling incident photons with electron density oscillations at metal-dielectric interfaces. This includes the wavelength and angle of the incident light beam, type and thickness of the metal layer as well as the refractive index of the two media.[89]

To excite PSPs, coupling light through a glass prism to a thin metal layer is the most common approach and was firstly shown by Otto, Kretschmann and Raether in 1968.[90,91]

There are two configurations taking advantage of attenuated total reflection (ATR) method[92]: Kretschmann and Otto geometry (see Figure 7). In the Kretschmann geometry, a high refractive index prism is attached to the backside of a noble metal layer. The *p*-polarized (transverse magnetically polarized, TM) light beam passing through is reflected on the base of the prism and generates an evanescent wave, which is penetrating the outer metal-dielectric interface. This field decays exponentially perpendicular to the surface and exhibits a penetration depth of around 100 nm.

In the Otto configuration, a dielectric layer separates the prism and the metal interface, allowing to measure thick layers. Since this gap is difficult to control, Kretschmann geometry is the preferred configuration in biosensing applications.

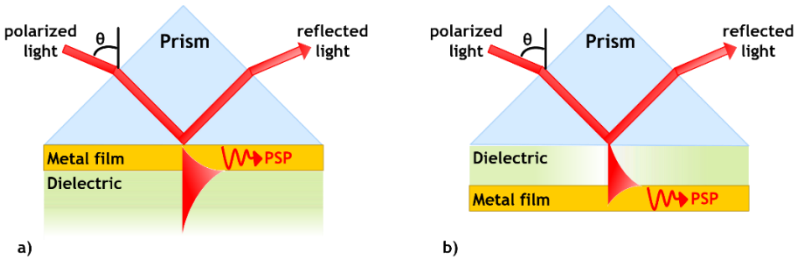

Figure 7: Coupling of light through the ATR method in two different geometries a) Kretschmann b) Otto.

Next to above mentioned configurations, light can also be coupled to surface plasmons by employing the diffraction on periodically corrugated metallic surfaces, so-called grating-couplers (see Figure 8). In contrast to ATR methods, this system is optically simpler, and advances in the fabrication of nanostructures on plastic substrates enabled the mass production of disposable and low-cost sensor chips.[93]

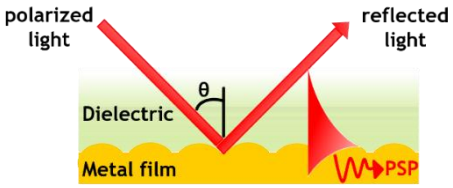

Figure 8: Grating coupler.

Molecular interactions on the sensor surface can be monitored via angular, wavelength and intensity modulation.[94,95] In devices using angular modulation of SPR, a monochromatic light beam is launched into the coupler and a photodetector detects the intensity of the reflected light in dependency of the angle of incidence $R(\theta)$.

In contrast to that in wavelength modulation, a polychromatic light source is coupled to PSPs at a fixed angle and a spectrometer detects the wavelength reflectivity spectrum $R(\lambda)$. In both cases, the reflectivity spectrum is measured and the position of the SPR dip minimum can be determined (see Figure 9a). Although those modalities usually give more accurate and precise information about the mass bound to the sensor surface, intensity modulation allows time-dependent monitoring and the direct detection of changes in refractive index units (RIU). The real-time kinetics $R(t)$ can be tracked by keeping both, the angle of incidence θ and wavelength λ at a fixed value. This value is usually chosen to be at the resonance edge where the reflectivity R shows the highest slope (see Figure 9b). This enables to determine reaction rates and thermodynamic properties of biomolecular interactions.[96]

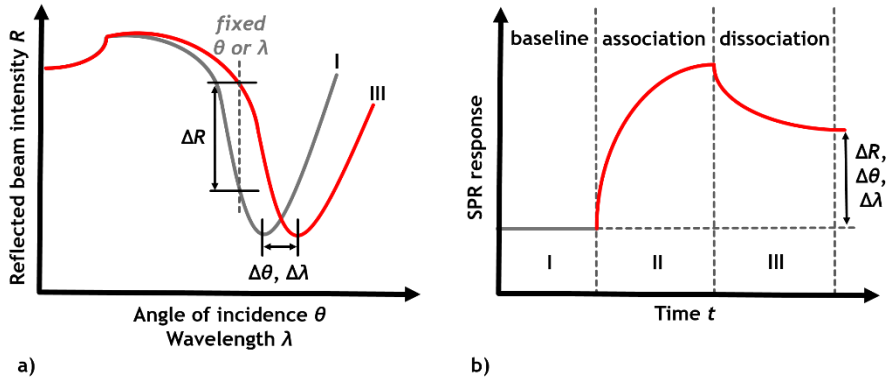

Figure 9: Sensing modalities in SPR sensing a) angular R(θ) and wavelength modulation R(λ) b) intensity modulation R(t) (based on figures in [89]).

Figure 10 shows a schematic of the interaction of a target analyte with an immobilized BRE on the SPR sensor. In a typical SPR measurement, a baseline response by flowing buffer over the functionalized biointerface is recorded (I). Association phase (II) starts when an analyte-containing solution gets in contact with the sensor surface. The interaction of the BRE and its analyte can be seen as a gradual increase in the SPR response (cf. Figure 9b), which reaches saturation. Rinsing the surface with buffer solution leads to a decreasing response through dissociation of the captured analyte (III). The recorded signal can be used to determine the association and dissociation constant of the analyte through fitting with an appropriate model. Since those experiments are usually performed in a flow cell, the analyte flow and diffusion conditions have to be taken into account.[96]

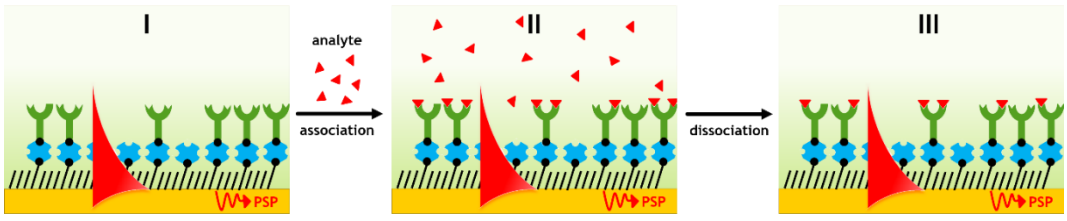

Figure 10: Biomolecular interactions showing the analyte association and dissociation on a functionalized plasmonic sensor surface.

Next to probing with PSP waves in the vicinity of the metal-dielectric interface, thin polymer layers attached to a metal surface (see Figure 11a) can support the guidance of optical waves in Kretschmann configuration.[97] To excite a dielectric waveguide, the refractive index of the polymer film has to be slightly higher than the one of the surrounding medium (e.g. buffer). Optical waveguide spectroscopy (OWS) can be used to determine the characteristics, like thickness and the refractive index, of an attached dielectric polymer slab (see Figure 11a), which can be 100 nm up to several microns thick. The reflection of light (see Figure 11b) on interfaces can be simulated using Fresnel equations.

Since regular SPR probes the sensor surface with only one mode (TM_0), the thickness (d_p) and the refractive index (n_p) of the attached layer (<1 µm) cannot be determined independently. With the appearance of additional waveguide modes (TM_1, TM_2,…), manifested as resonant dips in the angular reflectivity scans, a more detailed profile of the refractive index n_p of the attached layers can be assessed. Contrary to PSP resonances, optical waveguide resonances can also be excited through *s*-polarized (transverse electrically polarized, TE) light.

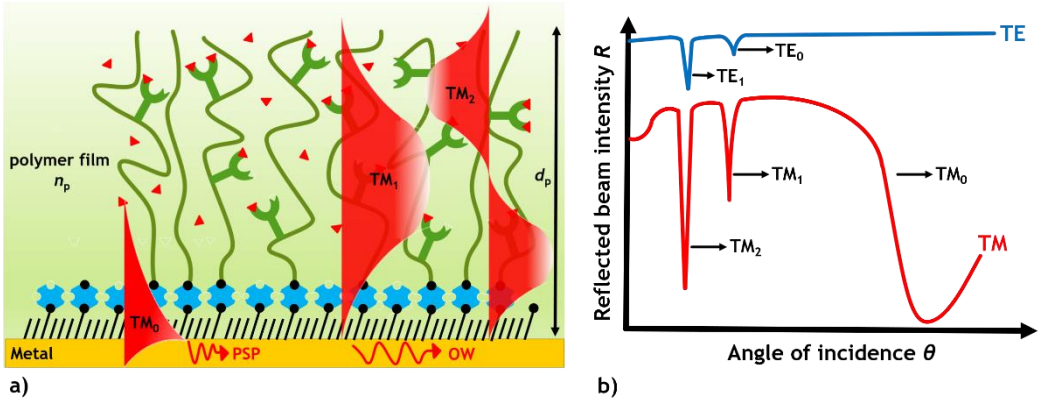

Figure 11: PSP and OW resonances a) on a plasmonic biosensor coated with a polymeric film b) reflectivity spectrum in TE (blue) and TM (red) mode (based on figures in [97]).

By analysing the reflectivity spectra $R(\theta)$, characteristics of the biointerface on the metal surface can be determined. This includes the thickness (d_p) and the refractive index (n_p) of the attached polymer layer, which is assumed to be a homogeneous bulk dielectric.

The surface mass density Γ of the attached layers can be approximated using the following equation.

$$\Gamma = d_{\mathrm{p}} \left(n_{\mathrm{p}} - n_{\mathrm{buffer}}\right) \frac{dc}{dn} \qquad (Eq.\,1)$$

where (dc/dn) ~ 5 mg/mm³ describes the change in refractive index with the concentration of organic material.[98]

2.3. Surface plasmon fluorescence spectroscopy

Fluorescence is a process of absorbing a photon at a certain excitation wavelength (λ_{ex}) followed by the re-emission at another wavelength (λ_{em}) as illustrated in the Jablonski diagram (see Figure 12).[99] Upon absorption, the fluorescent material is excited from its singlet ground (S_0) to an excited state (S_1-S_n), where it can exist in several different vibrational energy levels. Black arrows indicate the energy transition of a fluorophore in a free space while red ones those in the proximity of metallic surfaces.[92,100]

The spontaneous transition into the ground state is accompanied by radiative and non-radiative decay. The radiative decay involves the emission of photons at λ_{em} and can be detected in fluorescence measurements, considering that the lifetime of fluorescence is about 10 ns, for most of the common organic dyes. This emission occurs at lower energies (or longer wavelengths) and is referred to as Stokes Shift. Furthermore, it should be noted that the emission spectrum of fluorophores is strongly dependent on its chemical structure and the solvent in which it is dissolved.

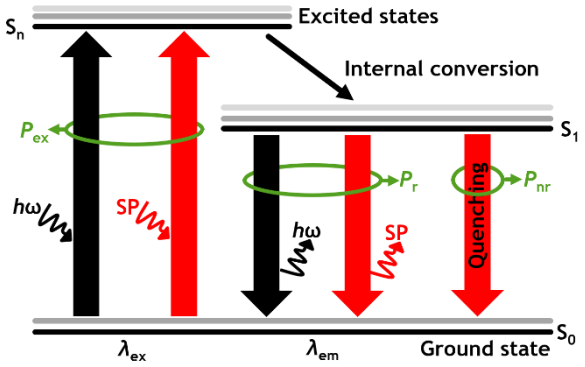

Figure 12: Jablonski diagram (based on figures in [92,100]).

By placing a fluorophore into the tightly confined electromagnetic field of PSPs, the large field intensity enhancement can increase the excitation rate. This coupling of fluorophores with PSPs is the bases of metal-enhanced (MEF) and surface plasmon-enhanced fluorescence (PEF), leading to increased fluorescence signals up to a 10^3-fold and higher quantum yields.[100] Contrary to radiative decay, non-radiative decay quenches the fluorescence signal at short distances (<15 nm) from metallic surfaces due to Förster energy transfer.[101] Through the energy transition of PSPs, the chromophores are excited by λ_{ex} and the fluorescence signal can be out-coupled into the far-field and detected at λ_{em}.

Figure 13a shows the fluorescence labeling of a bound analyte in an immobilization matrix. The surface plasmon coupled emission (SPCE) of fluorophores can be inversely seen in SPR reflectivity scans illustrated in Figure 13b.[102]

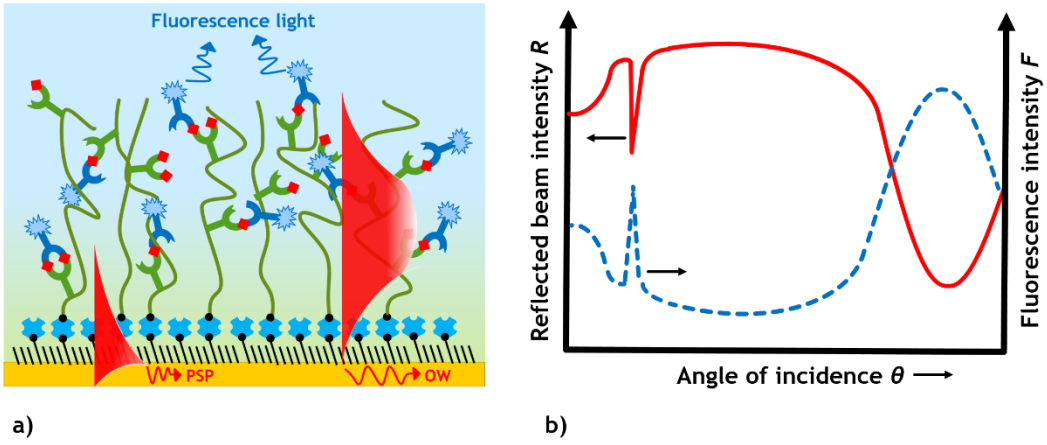

Figure 13: Fluorescence detection in SPFS a) plasmonic chip with a bound fluorescence label conjugate b) angular TM reflectivity spectrum (red-solid) and corresponding fluorescence intensity (blue-dashed).

In 2000, Liebermann and Knoll presented the first combination of SPR and surface plasmon fluorescence spectroscopy (SPFS) in Kretschmann configuration. They described the coupling regimes and distance dependencies of fluorophores on a plasmonic gold surface.[103] Three years later, they presented the detection of parallel multispot DNA hybridization events combining SPFS with surface plasmon resonance imaging (SPRi).[104] A comprehensive overview of biosensing applications can be found elsewhere.[105]

2.4. Sensor architecture and biointerface

The typical sensor chip for biosensing in Kretschmann configuration is a glass substrate coated with a thin layer of noble metal. Silver films usually yield the highest field intensities of resonantly excited PSPs.[106] Nevertheless, in biosensing applications, usually gold films are used to excite surface plasmons due to their chemically inertness and stability. Not only the type of material but also layer thickness, crystallinity and surface roughness of the deposited metal film plays an important role regarding the sensor's sensitivity.[107]

In general, there are several methods to deposit those thin layers, including thermal evaporation, sputter coating and template stripping. To stick gold to a glass substrate, an adhesive layer (usually chromium, titanium or metal oxides) is required.[108]
To produce a highly specific plasmonic biosensor, not only the chip's surface has to be optimized to get a sensitive signal. Also, the biointerface design and immobilization strategy of ligands and targets have to be selected according to the biosensors purpose.[72,109,110]

A plasmonic biosensor's specificity is mainly dictated by the surface architecture. For sensing in mixtures or complex matrices, containing several different molecules, the sensors biointerface needs to be highly controlled and designed to avoid unspecific adsorption of biomolecules to the metal layer.

Furthermore, one must consider that performed surface modifications are stable over time as well as under certain environmental and storage conditions.[111] Up to now, many strategies to create so-called anti-fouling/non-fouling surfaces have been established, which in a next step often allows to anchor BREs.

2.4.1. Self-assembled monolayers

Self-assembled monolayers (SAMs) are spontaneously formed ordered structures of organic molecules.[112,113] In SPR-based biosensing applications, gold is mostly functionalized with thiols or disulfides due to its capability to create strong and robust chemical bonds.

Thiol-terminated molecules, carrying oligoethylene glycol (OEG) head groups provide a good anti-fouling surface through creating a bioinert hydrophilic environment close to the surface.[114] Additional functionality of SAMs can be obtained by using mixed alkane thiols to introduce functional end groups, which in a next step can be utilized for covalent or affinity coupling of BREs (see chapter 2.5). Several groups investigated and optimized the ratio of those alkane thiols with respect to their length of the polymer chain.[115,116]

2.4.2. Polymer brushes

Polymer brushes serve a broad range of applications in nanotechnology due to their versatility of chain length, their controllable grafting density and chemical identity.[117,118] Due to their dense and branched structure, especially hydrogels have been used to prevent adsorption of proteins while simultaneously allowing a higher loading capacity of BREs in SPR biosensing. This immobilization matrix is especially favourable in biosensor applications when the analyte is relatively small (<10 kDa).[109] Another advantage of such 3D polymer matrices is the ability to design their response to external stimuli, e.g. solvent, pH, temperature and ionic strength, summarized in a review.[119]

Especially dextran-based coatings found daily application in commercially available sensor chips (CM5 from Biacore). This 100 nm thick polymer layer reduces non-specific binding and provides a binding matrix for analytes, which can be probed by evanescent waves.[120]

In general, polymer brush preparation can be classified into two approaches: “grafting-to” and “grafting-from.”[118,121] In grafting-to approaches, polymer attachment to a substrate is accomplished by appropriate end-functionalization of the polymer chains, which has been widely applied (e.g. fabrication of DNA microarrays).[122] This

method usually yields low grafting densities and thin polymer brush thicknesses. Due to this fact, grafting-from approaches are the preferred method to fabricate polymer brush architectures through surface-initiated polymerization (SIP) techniques. This allows to grow polymer brushes with high grafting densities from immobilized initiator monomers through SAMs and subsequent polymerization.

The conformation of polymer chains can be described by their end-to-end distance R_F (Flory radius) or by their radius of gyration R_g.[123] Surface-tethered polymer chains exhibit different conformations, depending on their grafting density σ (see Figure 14).[124,125] If the distance in between the grafting sites D is larger than R_g ($D > 2R_g$), the polymer chains do not overlap and take on a "mushroom"-like conformation. In contrast, at higher grafting densities ($D < 2R_g$), the adjacent chains start to repel and stretch away from the substrate. They take on a "brush"-like conformation with a polymer thickness $h > R_g$, measured as a distance between the vertically free end of brushes and the substrate. In summary, the thickness h of the polymer brush is dependent on the degree of polymerization N and an exponent v. This Flory exponent v is highly dependent on the grafting density σ as well as the solvent quality.[126]

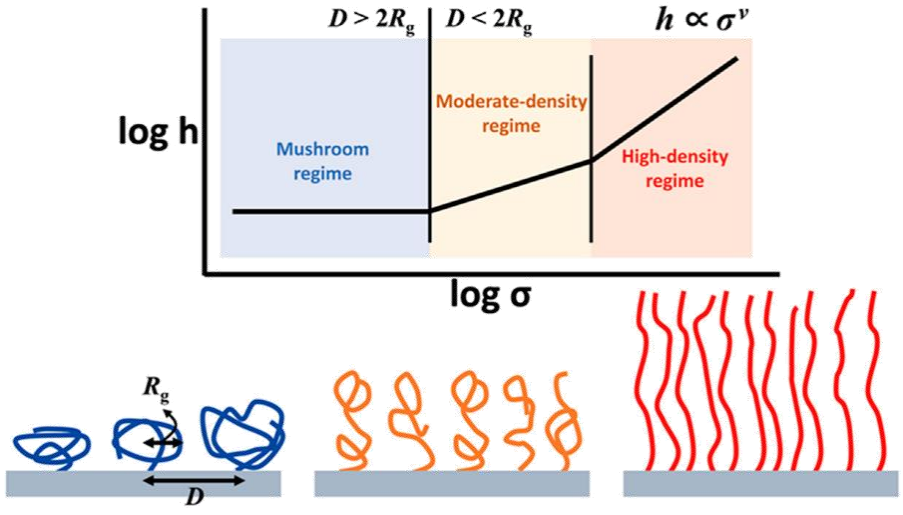

Figure 14: Schematic of different polymer brush conformations and their height h in dependency of their grafting densities σ on a solid support. (reprinted from [125])

2.5. Immobilization strategies

In SPR sensing, a huge variety of BREs can be immobilized to specifically detect target analytes.[127] Especially antibodies have been employed in the development of various medical diagnostic devices based on immunoassays. Although they offer means for the analysis of a wide range of biomarkers in disease detection, their production is expensive and functionalized sensors need special storing conditions in order to prevent protein denaturation.

In the past decades, the interest in constructing DNA-based sensing devices increased tremendously.[128] DNA-based BREs hold great potential for the detection of nucleic acid sequences, associated with inherited diseases, infectious pathogens as well as the development of cancer. Research in the development of nucleic acids gave rise to several synthetic DNA-based BREs, e.g. single-stranded DNA (ssDNA), peptide nucleic acids (PNAs), DNAzymes and aptamers. The latter are composed of functional nucleic acids, which give them a sequence-specific fold. Those engineered synthetic structures exhibit a tertiary structure and bind an extensive range of molecular targets, therefore achieving a more sensitive and selective detection of nucleic acids.

In general, BREs can be immobilized through physisorption (reversible) or actively through chemisorption (irreversible).[109] To efficiently couple a functional group to a surface, the following points should be considered. Non-covalent adsorption leads to a low number of active binding sites. Due to this fact, irreversible binding, through covalent binding, ensures consistent surface concentrations and is therefore the favoured method to immobilize BREs. Even if a densely immobilized BRE may increase the number of interactions and hence also the signal, steric hindrance and aggregation may block possible binding sites. Therefore, it is necessary to ensure availability and control the orientation of biorecognition molecules within the scope of biofunctionalization.[129] The following coupling techniques have been developed.

2.5.1. Covalent binding

Covalent binding describes the process of chemically joining two reactive groups.[130] Amine coupling is one of the most employed techniques to anchor proteins and peptides to reactive functional groups on the sensor's surface. This can be accomplished by reacting amino acids, which contain ionizable side chains as:

i. carboxylate groups (-COOH): aspartic and glutamic acid
ii. primary amine groups ($-NH_2$): lysine
iii. sulfhydryl groups(-SH): cysteine
iv. phenol groups: tyrosine
v. other groups: arginine, histidine, methionine, tryptophan

with chemical activated groups to form amide or amine bonds in acylation or alkylation reactions.

The most prominent covalent attachment is amine coupling via reactive esters.[109] Surface bound carboxylate groups (e.g. COOH-terminated SAM) are converted into a reactive ester, by carbodiimide [e.g. 1-Ethyl-3-(3-dimethylaminopropyl)carbodiimide (EDC)] activation. The unstable O-acylisourea intermediate can be stabilized by water-soluble N-hydroxysuccinimide (NHS) before an amide bond to primary amines of the BRE can be formed. An elaborate overview of additional coupling strategies and protocols can be found in several book chapters and handbooks.[109,130,131]

2.5.2. Affinity binding

Since the avidin-biotin bond is one of the strongest non-covalent bonds, it is widely used in sensor functionalization. The interaction between the tetrameric glycoprotein and the water-soluble vitamin shows a dissociation constant $K_d = 10^{-15}$ M.[132] The versatility of available biotin-modifications for BRE offers a wide range of applications and is used to either couple functional groups or detect target analytes.[133] Various bioassays exploit the affinity of biotin to avidin, streptavidin and neuravidin. Each of them harbours 4 binding sites, but they differ in their isoelectric points (*p*Is) and therefore prevent nonspecific binding to biointerfaces.

Especially because of its high mass (53-67 kDa), avidin binding to biotin moieties enables quantification of performed surface modifications or reactions in SPR biosensing.[134] Furthermore, two of its binding pockets are facing to the solution and therefore allow to attach BRE in a controlled and oriented manner. Su et al. described the immobilization of biotinylated DNA to a streptavidin film and investigated the impact on target DNA hybridization efficiencies.[135] They showed that streptavidin immobilization via a mixed thiol SAM containing biotin terminated headgroups created a more evenly distributed surface architecture. This led to better DNA hybridization efficiencies than on randomly oriented streptavidin films, obtained by amine coupling to COOH terminated headgroups.

Another way to immobilize immunoglobulins (e.g. IgG), is the affinity coupling of the heavy chain fragment via protein A or protein G. This coupling strategy is mostly used in immunosensor fabrication and has the advantage that sensors can be easily regenerated for several individual measurements on one chip.[109,136,137]

3. State of the art in biosensing using RCA

RCA has become a powerful tool to amplify the signal of a single binding event up to a 1000-fold and demonstrated to improve the sensitivity of nucleic acid based biosensors.[138] Various sensor platforms exploited this simple method to generate long ssDNA molecules to detect a broad collection of target analytes. Several strategies have been developed to visualize and quantify RCA products by optical or electronic means. Especially the combination of RCA with ligation-mediated padlock circularization (see 1.2.3) allowed single-molecule detection in multiplexed formats.

Lizardi et al. used fluorescence microscopy to visualize surface bound RCA products and distinguished amplification products using two different padlock probes.[139] They introduced fluorescein and Cy3 labelled detection oligonucleotides which allowed to specifically detect the condensed RCA products as single spots on a microarray.

In order to reduce the size of the generated RCA product of individual spots on a microarray, Clausson et al. presented a strategy which utilizes a compaction oligonucleotide to facilitate fluorescence imaging of RCA products.[140] This oligonucleotide was composed of two identical sequences, each of them complementary to a part of each tandem repeat of the RCA product. By including this compaction step, the local concentration of fluorophores was increased, which led to increased local fluorescence intensities and improved the signal-to-noise ratio.

Since RCA products tend to form random coils in the liquid phase, those formed DNA nanoclusters have also been detected by confocal microscopy in microchannels.[141]

Apart from taking advantage of the self-collapsing properties of DNA, long ssDNA strands have also been stretched over distances. Russell at al. showed that RCA products can be used to bridge electrode gaps over a distance of 5 µm.[67] Electrical detection was achieved by metallizing the RCA product with modified gold nanoparticles (AuNP) and subsequent determination of the sensors resistance. This technique allowed the detection of 10 ng of *E. Coli* genomic DNA.

3.1. RCA with circular padlock probes in SPR sensing

As already stated in section 2.2, the affinity capture of small analytes does not change the SPR signal sufficiently enough to detect low amounts of e.g. DNA molecules. Next to the detection with SPFS, signal amplification is also achieved through binding plasmonic nanomaterials, e.g. gold and silver particles to the target sequence. This leads to a great mass accumulation and induces additional RIU changes and has been mostly exploited in the detection of nucleic acids amplified through RCA on plasmonic structures.

Xiang et al. showed the isothermal amplification of padlock probes, complementary to five drug-resistance associated genes of *Mycobacterium Tuberculosis* in a mixture of wild-type and mutant genes (ratio 5000:1).[142] The padlock probes were hybridized with their target sequence and circularized by DNA ligase. Non-circularized padlocks and excess of linear oligonucleotides were removed by Exonuclease treatment. This removes unreacted probes, to prevent self-ligation amplification which may lead to a background signal reported by Hafner et al.[143] A thiolated DNA sequence served as capture probe on the SPR sensor surface, capable to basepair with a unique padlock sequence. They detected 8.2 pg/µL of genomic DNA in clinical samples by labelling the surface anchored RCA product with modified AuNP.

The same group improved the LOD even further by performing enzymatic steps, including ligation, RCA, exonuclease treatment and enzymatic cleavage of the RCA product ex-situ. Modified gold nanoparticles were directly assembled on the SPR sensor surface and captured the RCA cleavage products from clinical samples containing 10^4 CFU/mL in a label-free manner.[144]

Shi et al. connected the capture probe via biotin to streptavidin modified gold nanoparticles immobilized on the sensor surface.[145] Solid-phase RCA was initiated by hybridizing the circular padlock probe to the immobilized capture probe. They studied parameters like time and temperature on the hybridization efficiency of the padlock, RCA duration and the signal enhancement with modified AuNPs of different sizes and concentrations (15-30 nm). The sensitivity of the pursued assay was 0.5 pg/µL of genomic DNA.

Next to the detection of DNA hybridization events on plasmonic sensors, also aptamers have been utilized to detect the presence of human proteins using RCA as signal amplification strategy. He et al. detected thrombin with a LOD of 0.78 aM through ligation-mediated RCA of an aptamer-primer complex.[146] The generated ssDNA molecule was detected by a covalently attached hairpin aptamer on the SPR sensor. Subsequent labelling with DNA-barcoded nanoparticles gave a linear relationship detecting thrombin in the range from 10^{-18}-10^{-13} M. Atomic force microscopy (AFM) showed DNA strands up to a few micrometres. The sandwich-assay has also been performed on a QCM biosensor, giving comparable results.

However, in all detection strategies (surface anchored and liquid-phase RCA), they found that RCA duration above 40 minutes didn't increase the signal further. Possible explanations included limited polymerase activity, hybridization inhibition of detection probes due to steric hindrances of the generated RCA product or reached reaction equilibrium. Similar observations were also made by Huang et al., who reported the best amplification effects after 30 minutes of RCA development and subsequent labelling with AuNP (5 nm).[147] An overview of SPR sensors for the detection of bacterial pathogens was published by Taylor et al.[148]

Apart from the detection of target analytes, RCA has also been used to fabricate DNA polymer brush arrays, using photolithography as micropatterning technique.[149] Barbee et al. controlled the brush density by varying the concentration of circular template available for the immobilized DNA probes. Characterization of the RCA product was performed through fluorescence imaging, gel electrophoresis and atomic force spectroscopy (AFM). Although gel electrophoresis revealed the generation of long DNA strands (9 kilobases) within 2 minutes of RCA duration, AFM gave a height of only 12 nm.

4. Aim of work

Antibiotic resistance is a rising threat to global health. Current methods for the detection of antibiotic resistance are based on standardized testing procedures in microbial laboratories, which are time-consuming, expensive and tedious. This leads to over-prescription of broad-spectrum antibiotics which accelerates the evolvement of multi-drug resistant pathogens. Experts predict that by 2050 more people will die from antibiotic resistance than from cancer. This highlights the importance of new diagnostic tools to provide fast and reliable diagnosis, resulting in more efficient and less expensive treatment together with avoiding the misuse of antibiotics.

Molecular methods like real-time polymerase chain reaction (PCR) showed advances in the detection of antibiotic resistance on a genetic level. However, this method relies on multiple cycles of temperature changes to amplify DNA and the detection of multiple genes in one single test is limited to a few target genes. Although microarrays offer the detection of thousands of genes in a multiplexed format, DNA cross-hybridization often leads to false-positive results. However, the implementation of enzymatic steps as ligation-mediated padlock circularization in combination with on-chip rolling circle amplification (RCA) promises increased specificity and sensitivity in the detection of target genes.

SPR-based detection principles hold the potential to provide rapid means for the sensitive detection of biological analytes. Since a traditional SPR biosensor may not provide enough sensitivity towards the detection of DNA, the implementation of two different amplification strategies allows detecting target genes in an ultrafast and ultrasensitive manner.

Firstly, a ligation-based padlock probe concept is combined with RCA to amplify nucleic acids isothermally without using PCR. Secondly, the amplification product is detected by fluorophore labeling on a metallic thin film. Plasmonic amplification of fluorescence light enables to increase the fluorophore excitation by employing surface plasmon fluorescence spectroscopy (SPFS).

The specific goals of this thesis are related to the implementation of RCA on a plasmonic sensor (see Figure 15) and determining the following characteristics of this reaction.

I Speed of prolongation of nucleic acid strand on a solid support

II Control of the growth for longer strands by coupling the strand to the sensor surface, probed by the evanescent field of PSPs

III Formulate possible route for efficient implementation of the sensor platform using RCA for the rapid identification of antibiotic resistance genes in a multiplexed format

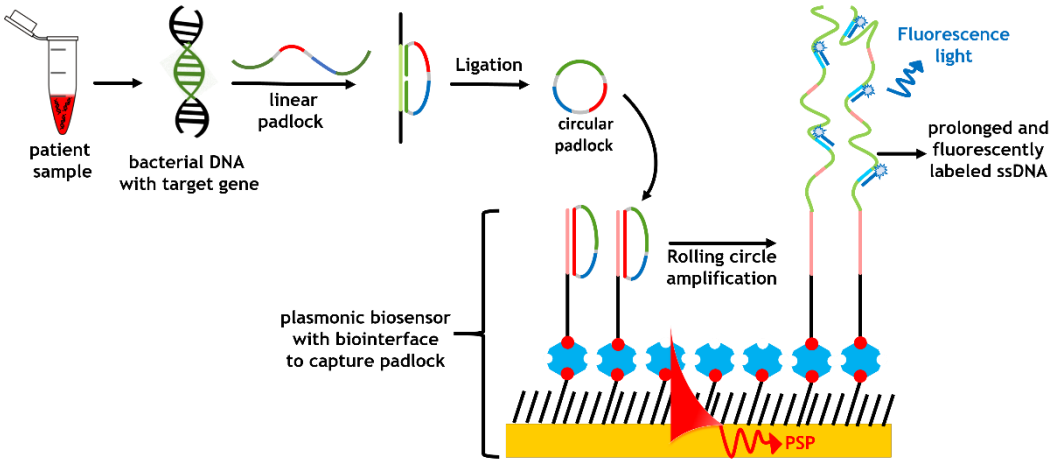

Figure 15: Schematics of the implemented assay on a plasmonic biosensor.

5. Materials and methods

5.1. Materials

The hydroxyl- (thiol-OEG-OH, HS-$(CH2)_{11}$-EG_6-OH, prod. No. TH 001-m11.n6) and biotin- (thiol-OEG-biotin, HS-$(CH2)_{11}$-EG_6-Biotin, prod. No. TH 004-m11.n6) terminated OEG thiols were purchased from ProChimia Surfaces.

Phosphate buffered saline (PBS, pH=7.4, cat. No. E504), nuclease-free water (NFW, cat. No. E476), Tween 20 (cat. No. 437082Q) and pure ethanol (cat. No. 1.11727) were obtained from VWR. Sodium chloride (NaCl, cat. No. S9888), calcium chloride ($CaCl_2$, cat. No. C1016), potassium chloride (KCl, cat. No. P9333), magnesium chloride ($MgCl_2$, cat. No. M8266) and sucrose (cat. No. S7903) were from Sigma Aldrich. Bovine serum albumin (BSA, cat. No. B9000S) was purchased from New England Biolabs.

Neutravidin (cat. No. 31050), phi29 DNA polymerase (ϕ-29 Pol, cat. No. EP0094), deoxy nucleoside triphosphates (dNTPs, cat. No. R0192), Exonuclease I (Exo I, cat. No. EN0581) and FastAP Thermosensitive Alkaline Phosphatase (cat. No. EF0651) were obtained from Thermo Scientific™ and Ampligase DNA ligase (cat. No. A3210K) from Epicentre.

DNA oligonucleotides, summarized in Table 1, were ordered from Integrated DNA Technologies and dissolved in nuclease-free water and stored at 4°C.

Table 1: Sequences of oligonucleotides used in this thesis: bold sequences, also named plus (+) sequences are complementary to their corresponding minus (-) sequences.

Oligonucleotide	**Sequence (5' → 3')**
Padlock probe **TS+/C2CA+/BS+/TS+**	/5Phos/**TGTGATACAGCTTTCTTGCGCGTGTATGCAGCTCCTCGAGTAGCCGCAGTTCG CGCCGCAGGGCCGATACGTGTAACTTAT**
TS-	/5Phos/AAGAAAGCTGTATCACAATAAGTTACACGTATCGG
Biotin/20T/TS-	/5Biosg/TTTTTTTTTTTTTTTTTTTTAAGAAAGCTGTATCACAATAAGTTACACGTATCGG
Biotin/20T/**TS+**/ dideoxy	/5Biosg/TTTTTTTTTTTTTTTTTTTT**CCGATACGTGTAACTTATTGTGATACAGCTTTCTT**/ 3ddC/-3'
Biotin/20T/BS-	/5Biosg/TTTTTTTTTTTTTTTTTTTTCTGCGGCGCGAACTGCG
Biotin/20T/**BS+**	/5Biosg/TTTTTTTTTTTTTTTTTTTT**CGCAGTTCGCGCCGCAG**
Biotin/20T/random	/5Biosg/TTTTTTTTTTTTTTTTTTTTCGACTACGACTACGACTAC
C2CA+/3'-Cy5	**GTGTATGCAGCTCCTCGAGTA**/3Cy5Sp/
5'-Cy5/random	/5Cy5/CAGCATCAGCTACGACTACGACTG

5.2. Methods

5.2.1. Optical set-up

The SPR set-up used for the measurements in this thesis (Figure 16) is a home-built instrument in Kretschmann configuration. The monochromatic beam of a Helium-Neon (He-Ne) laser (Lasos, LGK 7628, 350 µW/cm², λ_{ex} = 632.8 nm) passes through a laser-bandpass filter (LBPF, Thorlabs, FL632.8-10), a chopper (Signal Recovery, Model 197, frequency f = 933 Hz) and a polarizer. The incident beam is coupled to a 90° LASF9 glass prism (Schott, n = 1.850), which is optically matched to the sensor chip using high refractive index immersion oil (Cargille Laboratories; n = 1.7000, cat. No.1812) and is mounted on a rotation stage. The reflected beam intensity is detected by a photodiode connected to a lock-in amplifier (EG&G, Model 5210).

The transparent silica cover glass (Sico Technology) contains drilled in- and outlet ports and is clamped to the sensor chip using a PDMS gasket. The volume of the flow cell is 10 or 25 µL, for the regular and temperature-controlled SPR flow cell, respectively. The sample solution is flowed over the chip surface using a peristaltic pump and Tygon tubing (I_d = 0,25 mm) from Ismatec.

The emitted fluorescence light (λ_{em} = 670 nm) is collected by a lens (Thorlabs, focal length f = 50 mm, numerical aperture of NA = 0.2, LB1471), passed through a laser notch filter (LNF, Melles Griot, XNF-632.8-25.0M CVI) and two bandpass-filters (FBPF, Thorlabs, FB670-10 and Andover Corporation Optical Filter, 670FS10-25) before it is collected by a second lens and delivered to a photomultiplier (Hamamatsu, H6240-01) and a photon counter (Agilent, 53131A, f = 225 Mhz). If necessary, a neutral density filter (Thorlabs), to reduce bleaching of fluorescence dye molecules was applied. The fluorescence intensity F [(in counts per seconds (cps)] and the reflected beam intensity R in % is recorded by using the Software Wasplas (developed at Max Planck Institute for Polymer Research in Germany) as a function of time $R(t)$ or angle of incidence $R(\theta)$.

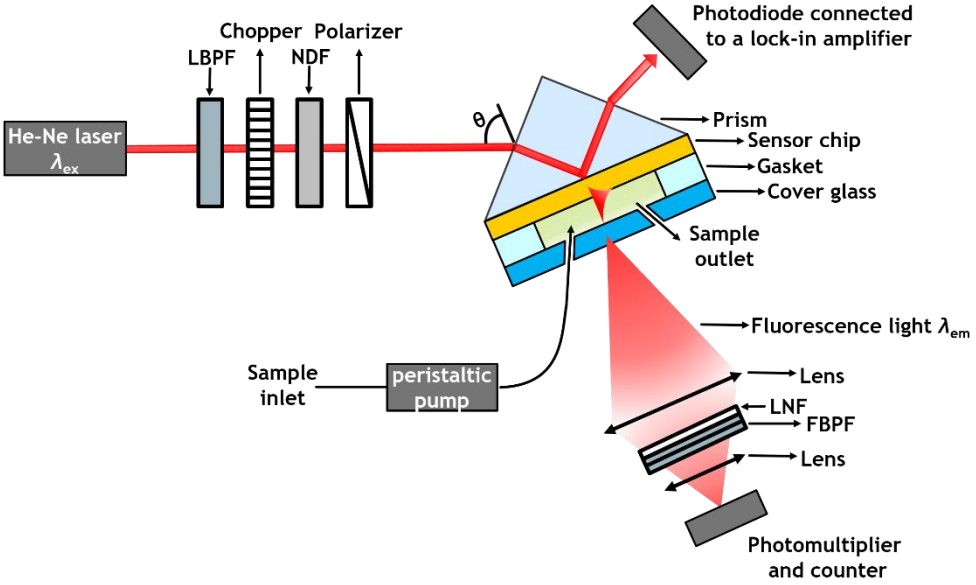

Figure 16: Schematic of the used SPR set-up in Kretschmann geometry in combination with surface plasmon fluorescence spectroscopy (SPFS).

5.2.2. Chip production and self-assembled monolayer

BK7 or LasF9 glass substrates (2 x 2,6 cm) were sonicated for 15 minutes in 1% Hellmanex (Hellma Optics) in MilliQ water (R ≥ 18.2 MΩ/cm²), MilliQ and Ethanol respectively. The substrates were rinsed with pure ethanol and dried with pressured air before they were loaded into a vacuum thermal evaporator (HHV Ltd, Auto306 Lab Coater). 2 nm of chromium (MaTeck, cat. No. 009540) and 50 nm of gold (MaTeck, cat. No. 900426) were deposited at a pressure lower than 10^{-6} mbar.

SAMs were formed by subsequent immersion in a 1 mM ethanolic solution, containing a mixture of OEG-thiols. The molar ratio of thiol-OEG-biotin and thiol-OEG-OH was 1:4. After incubation overnight the chips were rinsed with pure ethanol, dried under a nitrogen stream and stored in the dark in an argon atmosphere.

5.2.3. Experimental workflow and assay conditions

All solutions were continuously flowed over the sensor chip at room temperature and the flow rate was set to 50 µL/min. To save reagents, the reaction mixtures, containing proteins and enzymes, were continuously reintroduced by closing the tubing loop.

Neutravidin immobilization

Neutravidin (1.87 µM or 125 µg/mL) in PBST [0,05% (v/v) Tween20 in nuclease-free PBS] was flowed over the chip until saturation (20-90 minutes).

Primer immobilization

The biotinylated primer sequence (biotin/20T/BS- or biotin/20T/BS+) was reacted with the immobilized neutravidin at a concentration of 40 nM in PBST until saturation (30 minutes).

Ligation without exonuclease treatment

For the ligation reaction 40 nM of the target sequence (biotin/20T/TS-) were hybridized with 90 nM of padlock and 75 Units of Ampligase in NFW-BSA (0.2 mg/mL) in the respective buffer (20 mM Tris-HCl, 25 mM KCl, 10 mM $MgCl_2$, 0.5 mM NAD, and 0.01% Triton® X-100) in a total volume of 500 µL. The mixture was incubated ex-situ on a shaker (Eppendorf Thermomixer comfort) for 1 hour at 50°C at 700 rpm, if not stated otherwise. In order to inactivate the ligase, the mixture was heated up to 85°C for 5 minutes.

DNA denaturation was performed at 95°C for 5 minutes before the reaction mixture was immediately chilled on ice to prevent re-hybridization of the DNA strands. This step was performed, if it was decided to bind the padlock to an immobilized primer sequence, which was pre-reacted with neutravidin.

To establish the respective buffer conditions and determine the RIU change of the ligase buffer on the chip, 75 Units of Ampligase in the corresponding buffer in NFW-BSA were treated the same way as described above. Immobilization of the biotin/20T/TS-|padlock mixture was performed until saturation (30 minutes).

Ligation with exonuclease (Exo I) treatment

For the ligation reaction 8 or 80 nM target sequence (TS-) was reacted with 180 nM padlock and 75 Units of Ampligase in NFW-BSA (0.2 mg/mL) and the respective buffer (20 mM Tris-HCl, 25 mM KCl, 10 mM MgCl2, 0.5 mM NAD, and 0.01% Triton® X-100) in a total volume of 250 µL. The mixture was incubated ex-situ in a shaker for 2 hours at 50°C at 700 rpm and heated up to 85°C for 5 minutes to inactivate the ligase.

Subsequently, 50 Units of Exonuclease I, 5 Units of Alkaline Phosphatase in the respective buffer (67 mM glycine-KOH, 6.7 mM $MgCl_2$, 1 mM DTT) were added to the ligation mixture and filled up to a total volume of 500 µL with NFW. The mixture was incubated for 15 minutes at 37°C at 700 rpm to remove unligated padlocks and the linear target sequence before the Exonuclease was inactivated at 85°C for 15 minutes.

In order to bind the padlock to the neutravidin monolayer, the reaction mixture was pre-reacted with 10 µL of 40 nM of biotinylated primer sequences (biotin/20T/BS-, TS+, random) and incubated at room temperature for 15 min on a HulaMixer (Thermo Fisher Scientific). The baseline prior and after immobilization was established with the same enzyme mixture in the absence of DNA oligonucleotides.

Rolling circle amplification

Rolling circle amplification was conducted with 100 Units of ϕ29-Pol and 100 µM of each dNTPs in the respective buffer [33 mM Tris-acetate, 10 mM Mg-acetate, 66 mM K-acetate, 0.1% (v/v) Tween 20, 1 mM DTT] in a total volume of 500 µL in NFW-BSA (0.2 mg/mL).

Prior RCA the chip was rinsed with RCA buffer in NFW-BSA. To terminate RCA, the sensor surface was rinsed with RCA buffer and PBST.

Labelling with fluorescently labeled oligonucleotides

In order to be able to compare fluorescence intensities on different chips, the fluorescence intensities were normalized with that measured for the bulk response (prior to RCA) of 2.5, 5 and 10 nM C2CA+/Cy5 in PBST.

For RCA product labeling, the labelled oligonucleotide was hybridized at a concentration of 10 nM for 10 minutes before the surface was rinsed with PBST for 5 minutes and the fluorescence signal (Δ*F*) was determined.

Data acquisition and analysis

Routine SPR measurement started with recording a reflectivity spectra *R*(θ) of a bare gold chip in the angular range from θ = 45-60° in PBST buffer.

Time-dependent *R*(*t*) kinetic measurements were performed at a fixed angle, where the reflectivity scans showed a linear slope of *R*(θ) (low-angle side of resonance dip). A baseline in degassed PBST buffer was recorded, before sucrose of different concentrations (0, 1, 2 and 4% (w/v) in PBST) with *n* = 1.3330, 1.3344, 1.3359, 1.3388 refractive index unit (RIU) were flowed over the chip.[150] The SPR sensor response *R*(*t*) was normalized to the change in bulk refractive index and converted into Δ*R*(*t*) in mRIU, after setting the baseline response in PBST to zero.

After each immobilization or reaction step (neutravidin, primer, padlock, RCA), the sensor surface was rinsed with PBST and an angular reflectivity spectrum *R*(θ) was recorded. The curves were fitted using Winspall, a software based on Fresnel reflectivity-based models, developed at Max Planck Institute for Polymer Research in Germany.

The thickness *d* of each immobilized layer was determined by analysing the shift of the resonance angle. Parameters of materials and layers on the sensor chip were taken from literature and the values were converged to those summarized in Table 2.[151] It should be noted, that the thickness *d* and the complex refractive index *n* of the metallic layers, showed small variations, due to differences in chip production in each evaporation batch.

Table 2: Thickness d and complex refractive index n of layers on the sensor chip.

layer	*d* (nm)	Complex refractive index *n*
glass	-	1.845
chromium (Cr)	2	3.1 + 3.3i
gold (Au)	50	0.2 + 3.5i
SAM	1	1.45
neutravidin	determined	1.45
primer and padlock	determined	1.45
RCA product	determined	1.45 or determined

PBST (buffer)	-	1.333

The surface mass density Γ (ng/mm²) for each immobilized layer was determined using the following equation.

$$\Gamma = d_{\text{layer}} \left(n_{\text{layer}} - n_{\text{buffer}}\right) \frac{dc}{dn} \qquad (Eq. 1)$$

The incremental change in refractive index with the concentration (dn/dc) is very similar for protein and DNA and therefore was set to a value of 0.2 mm³/mg.[152,153] The appearance of additional optical modes during and after RCA allowed to reveal a more detailed refractive index profile of the DNA strands, which was dependent on the grafting density and conformation of the generated DNA brush in individual measurements.

The surface mass density Γ (ng/mm²) of the immobilized neutravidin and primer|padlock layer was converted into a grafting density σ (in nmol/mm²) by using their respective molecular weights (Table 3). This data allowed to assess the binding ratio of the primer|padlock duplex to the neutravidin layer.

Table 3: Molecular weight of neutravidin and used DNA oligonucleotides.

Layer	molecular weight *M* (kDa)	number of nucleotides (nt)
neutravidin	67	-
biotin/20T/TS-	17	55
biotin/20T/BS-	12	37
padlock probe	25	81

To estimate the length of each individual grown DNA strand, the generated surface mass density Γ was divided by the grafting density σ of immobilized padlock probes. This allowed to convert the mass increase per oligonucleotide strand in Dalton (Da) into number of padlock turns and in the next step into number of nucleotides.

6. Results and Discussion

6.1. Experimental design

In this thesis, the DNA sequence *bla*$_{OXA-48}$, which encodes for a *β*-lactamase in bacterial species, has been chosen to serve as the target sequence. To sensitively detect the presence of the target sequence, a single-stranded padlock probe OXA-48 (see Figure 17) was designed by a collaborator (Ivan Barišić, AIT, HMD). The specificity towards *β*-lactamase encoding gene segments in clinical isolates was successfully shown in a 100-plex reaction on microarrays.[64,154] The 81 nucleotide (nt) linear synthetic DNA strand is composed of three different segments, each of them having a specific function. DNA segments containing sequence marked with a plus (+) strands are complementary to their corresponding minus (-) strands.

The 3' and 5'-target recognition arms containing the TS+ sequence can hybridize to the target sequence (TS-). The C2CA+ sequence provides a repetitive sequence for RCA product labeling. The unique barcode sequence (BS+) is used to bind the padlock to the sensor surface and allows to detect different padlock probes in future multiplex reactions.

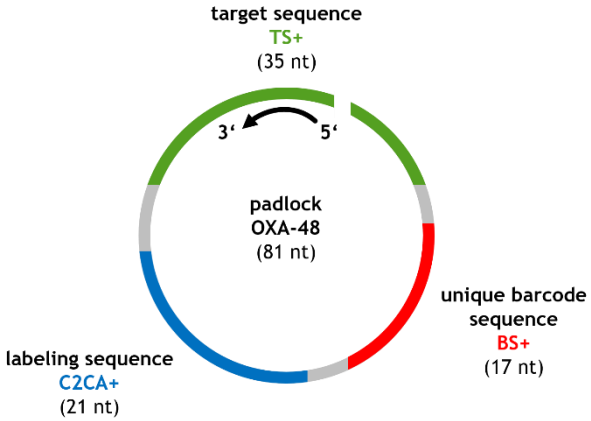

Figure 17: Schematic of the padlock probe OXA-48 containing three sequence specific regions: the 5' and 3' target recognition arms (TS+, green) are complementary to the target sequence (TS-), the labeling sequence C2CA+ (blue) provides a repetitive sequence for fluorescence labelling after RCA and a unique barcode sequence BS+ (red) to bind the padlock probe to the sensor surface and provide means for multiplex detection.

As illustrated in Figure 18, a synthetic DNA strand containing the target sequence (TS-, light green) served as the model analyte and was incubated ex-situ with the padlock probe. Upon hybridization, the artificial nick in the padlock probe is sealed during enzymatic ligation which results in circularization of the padlock probe.

The molar concentration of the padlock was chosen to be in excess of the target sequence (TS-). Due to this fact, unligated padlock probes and the linear target sequence were removed by Exonuclease I (Exo I). This enzyme catalyses the degradation of linear single-stranded DNA in the 3' to 5'direction and should prevent self-ligation amplification products or other side reactions, which may lead to a background signal.[143]

For sensor fabrication, custom cut glass slides were coated with 2 nm of chromium and 50 nm of gold. The gold sensor surface was modified with a mixed thiol SAM and the molar ratio of antifouling thiol-OEG-OH and thiol-OEG-biotin was adjusted to 4:1 respectively. The biotin groups served as a linker for neutravidin to provide a highly controlled biointerface for subsequent primer and padlock immobilization.

The biotinylated primer sequence (biotin/20T/BS-) was designed to be complementary to the unique barcode sequence (BS+) on the padlock and contains a set of repetitive thymine nucleotides (20 T). This spacer sequence should ensure better padlock hybridization and prevents fluorescence quenching close to the metal surface.

Upon binding of the ligated, circularized padlock probe the sensor surface, RCA was initiated to generate long single-stranded DNA strands containing multiple repeats complementary to the padlock sequences (BS-, C2CA-, TS-). This reaction is catalysed by a ϕ29-DNA-polymerase, which sequentially incorporates nucleotides (dNTP's). All experiments were carried out at room temperature.

SPR detection principle allowed online monitoring of each immobilization step and to determine the surface mass density of bound molecules by fitting $R(\theta)$ with a Fresnel-based reflectivity model. The PEF module was used to monitor the affinity binding of fluorophore-labelled oligonucleotide strands (C2CA+/Cy5). The change in fluorescence intensities ΔF was determined as the signal difference before injecting the fluorophore-labelled sequences (10 minutes) and after 5 minutes of rinsing with buffer.

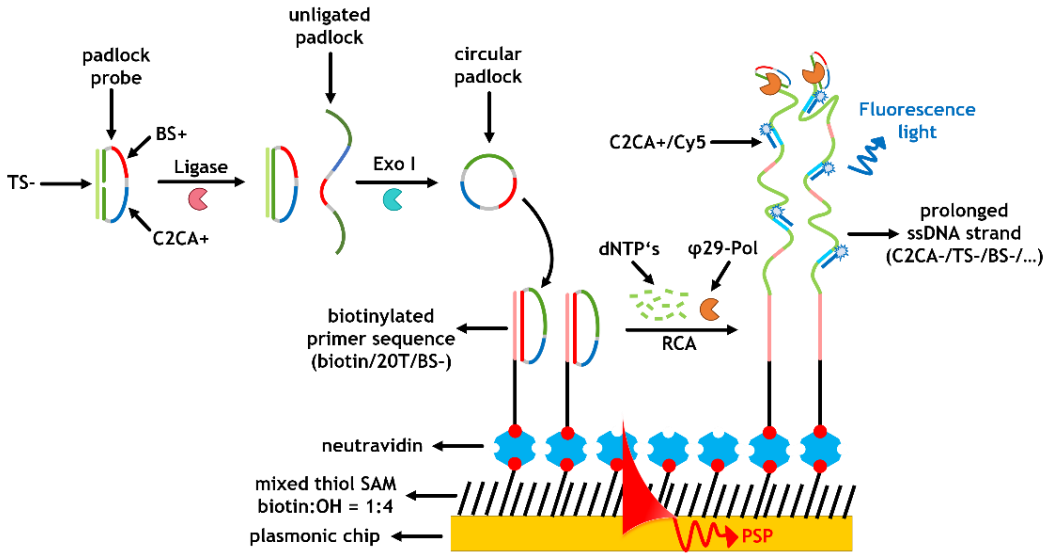

Figure 18: Detection of the synthetic target sequence (TS-) based on ligation-mediated padlock circularization, Exonuclease I treatment and subsequent detection with rolling circle amplification (RCA) on a plasmonic sensor with SPFS readout.

6.2. Liquid phase RCA

To verify the assay concept and check the activity of used enzymes, all enzymatic steps were performed ex-situ in Eppendorf tubes, as stated in the methods section "Ligation with exonuclease (Exo I) treatment". As illustrated in Figure 19, the synthetic target sequence (TS-) was reacted with the padlock probe in a ligation reaction, before unligated padlock probes and the linear target strand (TS-) were removed by Exonuclease I (Exo I). The ligated padlock was hybridized with a biotinylated complementary sequence (biotin/20T/TS-, 55 nt) before RCA was conducted in the liquid phase on a shaker for 1h at room temperature. To validate the performance of the pursued assay, mixtures after each enzymatic reaction step were analysed by agarose gel electrophoresis.

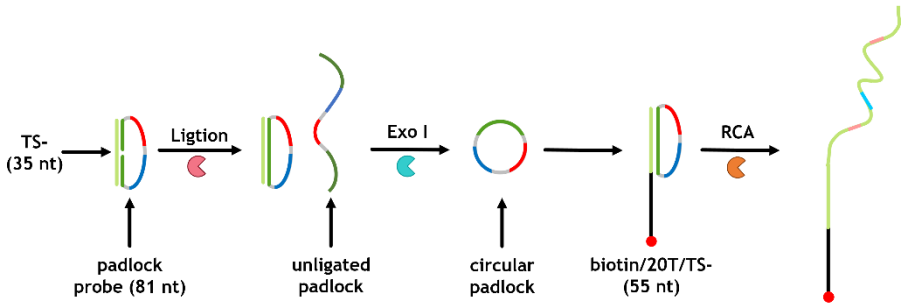

Figure 19: Schematic of the pursued assay for liquid phase RCA.

Agarose gel electrophoresis (see Figure 20) revealed the activity and specificity of all enzymatic steps and separated the DNA oligonucleotides based on their size. The 35 nucleotide (nt) long synthetic target sequence (lane 4) migrated faster than the 81 nt long padlock probe (lane 3) and the padlock hybridized to the target sequence (116 nt). Exo I treatment lead to the removal of linear oligonucleotides (lane 9 and 10). The circular padlock probe was not degraded by Exo I (lane 7). The difference in band intensities can be attributed to different concentrations of DNA oligonucleotides as well as dilution of the reaction mixtures.

The dark band in lane 11 represents the RCA product. The length of the DNA fragment in the lower band was estimated to be ~20 kilobases (kb), which proved that ϕ29-Pol could amplify the sequence of the padlock at least 250 times, with a speed of ~330 nucleotides per minute (nt/min) at room temperature. Some RCA products exceeded the length of DNA products and could not enter the 1% agarose gel and are visible as a band in the loading well. The lower band in lane 11 is the 55 nt long primer sequence, which has not been elongated at its free 3'-OH group.

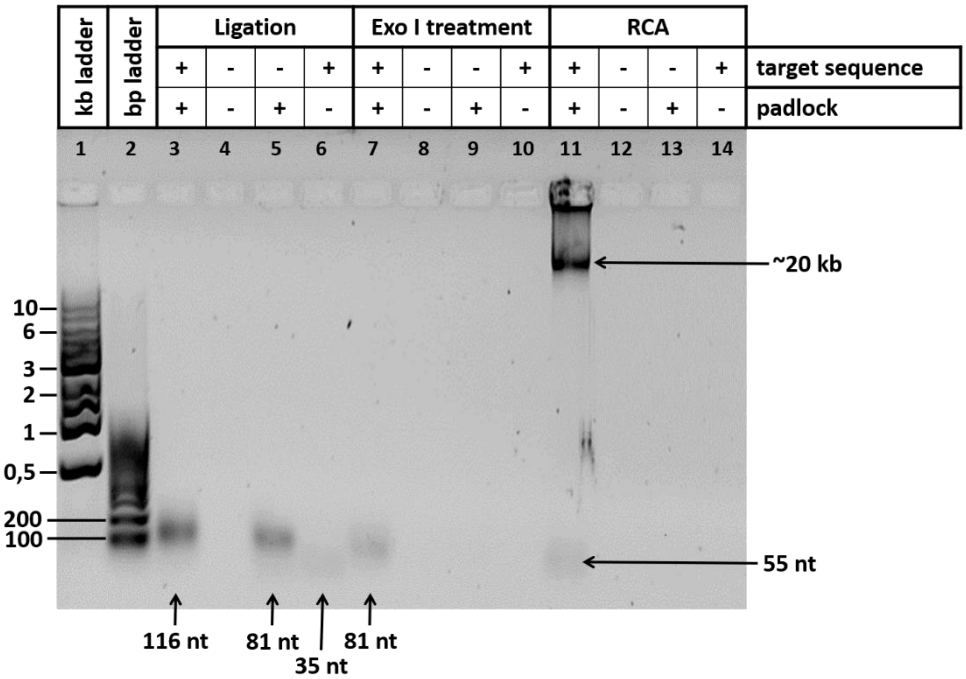

Figure 20: Image of an agarose gel (1% Agarose, stained with SYBR Green, 100 V, 1h) of reaction mixtures after different enzymatic steps. The plus (+) and minus (-) symbols present the absence or presence of DNA sequences. Lane 1, 1 kb DNA-ladder; Lane 2, 100 bp DNA ladder; Lane 3, ligated padlock hybridized with the target sequence (padlock/TS-), Lane 4, control well (Ligation buffer); Lane 5, target-free ligation product (padlock); Lane 6, padlock-free ligation product (TS-); Lane 7-10, Exonuclease I treated samples from Lane 3-6; Lane 11-14, RCA products from Lanes 7-10.

6.3. Implementation of RCA on a solid support

6.3.1. Specificity of fluorophore labeling

As a next step, the assay (depicted in Figure 21) was implemented on a plasmonic chip with combined SPR and SPFS readout.

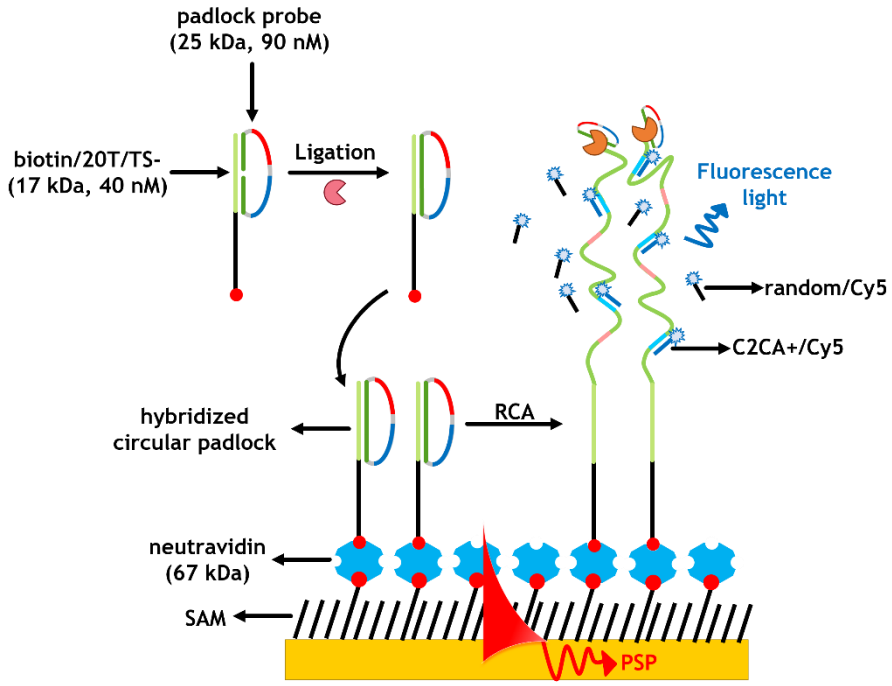

Figure 21: Reaction scheme of the pursued assay with two different fluorophore-labeled oligonucleotides: complementary C2CA+ (blue) and non-complementary, randomized control sequence (black).

Figure 22 shows a typical kinetic R(t) measurement of the pursued assay on the sensor surface in a flow cell containing 25 µL of sensing volume. Firstly, the mixed thiol-SAM modified sensor surface was reacted with neutravidin (NA). The affinity binding of neutravidin to biotinylated head groups of the SAM showed a reaction saturation at ΔR_{NA} = 4 mRIU.

PBST rinsing was followed by rinsing the sensor chip with ligase in its recommended buffer. The abrupt jumps in the SPR response when introducing the ligation and RCA buffer are explained by the difference in their bulk refractive index, due to different buffer compositions.

For proof of concept, the padlock probe was incubated with the biotinylated target sequence (biotin/20T/TS-) and ligated ex-situ for 1h (see Ligation without exonuclease

treatment). It was assumed that every hybridized padlock probe got circularized, which allowed skipping Exonuclease I treatment. The ligation product (circularized padlock hybridized to biotin/20T/TS-) was immobilized via affinity binding to neutravidin and lead to a change in sensor response of $\Delta R_{\text{biotin/20T/TS-|padlock}} = 1.2$ mRIU.

All immobilization steps based on the affinity binding of neutravidin to biotin showed saturation within 20 minutes in all performed experiments.

RCA was initiated by the addition of ϕ29-Pol and dNTPs. The linear increase in the sensor response corresponds to the binding of polymerase and the gradual linear assembly of the ssDNA strands. The reaction was terminated by removing dNTPs by injection of RCA buffer after one hour of reaction and rinsing with PBST buffer. The change in refractive index was $\Delta R_{\text{RCA}} = 2.3$ mRIU.

To confirm that the fluorescence signal is only present after RCA, complementary (C2CA+/Cy5) and a non-complementary, randomized Cy5 labeled (random/Cy5) oligonucleotides were introduced after each immobilization step.

As seen in Figure 22, the fluorescence intensity *F* increases abruptly after fluorophore injection. This is due to the excitation of the Cy5 fluorophores in the bulk solution. The bulk excitation intensity of C2CA+/Cy5 and random/Cy5 was 2900 and 2200 cps, respectively. In the case of fluorophore injection before RCA, the *F*-signal dropped back to the baseline, which confirmed that the labeled oligonucleotides did not bind to the sensor surface. Contrary to that, after pursuing RCA, affinity binding of random/Cy5 was observed giving a sensor response $\Delta F_{\text{random}} = 600$ cps. Nevertheless, a 130-fold stronger response ($\Delta F_{\text{C2CA}} = 80{,}000$ cps) verified the high affinity of C2CA+/Cy5 to the generated RCA product.

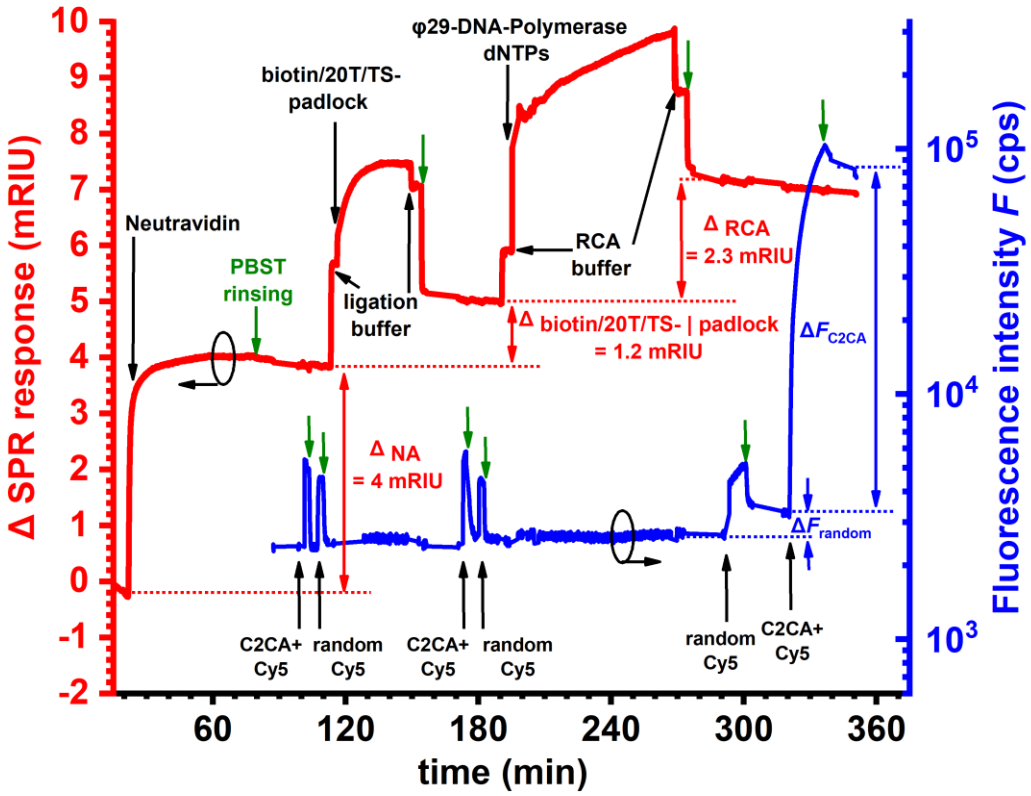

Figure 22: R(t) at a fixed angle in a flow cell containing a sensing volume of 25 µL, change in SPR response (red) and fluorescence intensity (blue).

Angular reflectivity scans $R(\theta)$ after each assay step allowed to obtain the surface mass density Γ of the surface-bound molecules after PBST rinsing. The curves in Figure 23 were analysed as described in "Data acquisition and analysis" and the obtained values of the generated biointerface are presented in Table 4.

Table 4: Characteristics of the generated biointerface containing ssDNA brushes in PBST buffer (n = 1.333).

	d **(nm)**	***n*** **(RIU)**	**Γ (ng/mm²)**	**σ (10^{-5} nmol/mm²)**
neutravidin	3.80	1.45	2.2	3.3
biotin/20T/TS- | padlock	0.88	1.45	0.5	1.2
RCA (1h)	1300	1.3352	14.3	

The obtained values for the neutravidin layer correspond to a monolayer with two binding pockets facing to the solution.[152,155] At a full surface coverage, the bound proteins with dimensions of ~5.6 × 5 × 4 nm[156] show a ~7 nm centre-to-centre distance.[157] Having a closer look the grafting density σ of the biotin/20T/TS-|padlock duplex revealed that only one third of the neutravidin molecules carried an

oligonucleotide strand. This is not surprising when taking into account that the diameter of the circular 81 nt long padlock probe can be estimated to be ~10 nm.[158]

After 1h of RCA and C2CA+/Cy5 labeling the appearance of an additional feature close to the critical angle (θ_c) in Figure 23 shows the appearance of a waveguide mode (TM_1) which is manifested as dip in the fluorescence intensity $F(\theta)$. This observation allowed to determine the refractive index n_{RCA} = 1.3352 as well as the thickness of the surface-bound RCA product and revealed that the ssDNA strands formed a d_{RCA} = 1.3 µm thick polymer layer. The emitted fluorescence intensity probed by the PSP mode was substantially higher than the one probed by TM_1 and showed that the majority of the Cy5 fluorophores were excited by the exponentially decaying evanescent field close to the sensor surface.

Assuming that each of the immobilized padlocks was elongated by ϕ29-Pol, the mass of the generated RCA product per immobilized padlock probe was estimated. For the given values, a mass of ~940 kDa per oligonucleotide strand was determined, which equals to a length of 3,000 nucleotides. This indicates that the padlock probe (81 nt, 25 kDa) had been amplified ~37 times with a speed of ~50 nt/min.

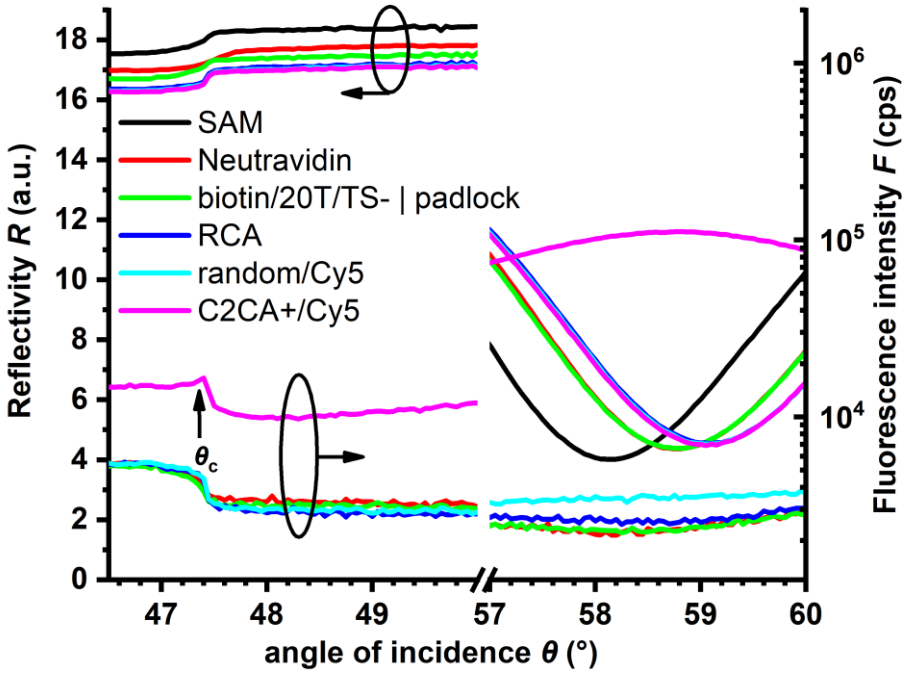

Figure 23: R(θ) after each immobilization step, followed by introducing Cy5 labeled oligonucleotides.

6.3.2. Specificity of padlock hybridization

Next to the specificity of the ligation reaction, which ensures the circularization of the padlock, the specificity of the pursued assay also depends on its hybridization to the chip surface. To test if RCA can only be pursued when the circular padlock is hybridized to the sensor surface, the following experiment has been performed (depicted in Figure 24).

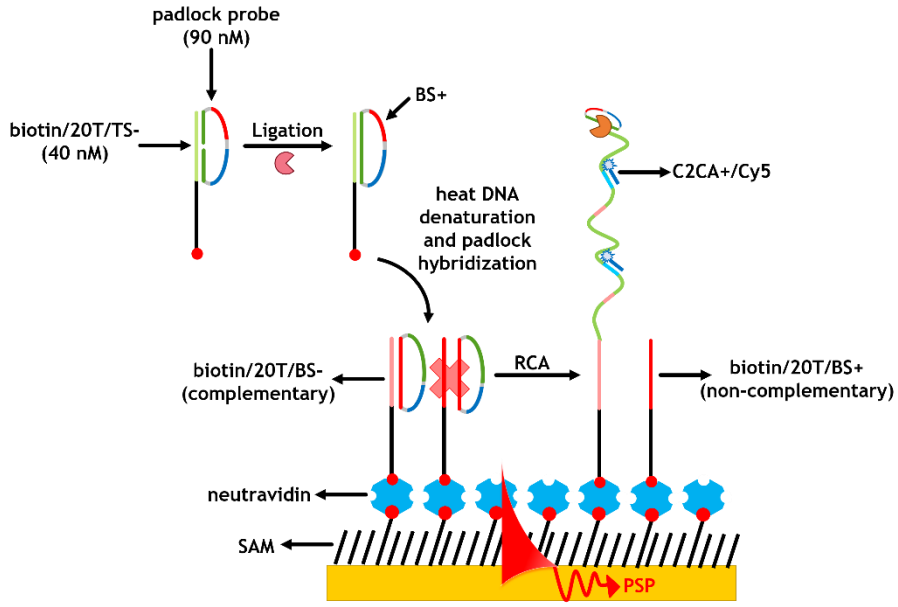

Figure 24: Assay scheme to test padlock binding specificity on the sensor surface. Ligation of the padlock was conducted in the presence of the biotinylated target sequence (biotin/20T/TS-), the formed DNA duplex was denatured by heat and let hybridized to a plasmonic sensor containing either the padlocks complementary primer sequence (biotin/20T/BS-, rose) or a non-complementary control sequence (biotin/20T/BS+, red). Initiation of RCA could only generate surface bound ssDNA strands, if the padlock was hybridized with its barcode sequence (BS+) to its corresponding primer sequence (biotin/20T/BS-)

The kinetic measurement *R*(t) in Figure 24 shows the affinity binding of two different biotinylated DNA sequences (see Primer immobilization) to individual neutravidin (ΔR_{NA} = 4.05 ± 0.1 mRIU) coated sensor chips.

(i) biotin/20T/BS- (black) primer sequence (complementary to padlock's BS+)

(ii) biotin/20T/BS+ (red) control sequence (non-complementary to padlock)

The padlock probe has been ligated as stated in the materials section (Ligation without exonuclease treatment) and was denatured by heat before the mixture was flowed over the sensor surface.

As seen in the black SPR curve in Figure 25, RCA could only be pursued if the circular padlock probe (containing BS+) was hybridized to its complementary primer sequence

(biotin/20T/BS-), which manifested as an association curve after RCA initiation. The generation of RCA product lead to change in refractive index $\Delta R_{\text{RCA-biotin/20T/BS-}}$ = 1.82 mRIU. In contrast to that, the red SPR curve dropped back to the baseline level (of $\Delta R_{\text{RCA-biotin/20T/BS+}}$ = -0.23 mRIU) upon PBST rinsing after 1 hour of RCA. This confirmed that the heat-denatured single-stranded padlock did not bind to the immobilized non-complementary (biotin/20T/BS+) control sequence and hence no surface-bound RCA product could be generated.

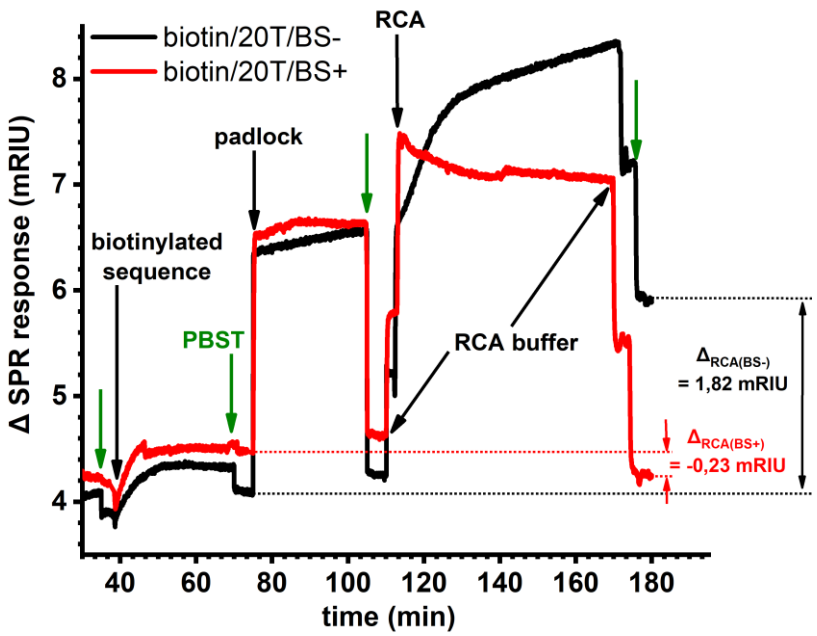

Figure 25: Kinetic measurement R(t) of pursued immobilization steps in a flow cell containing a volume of 25 µL on a neutravidin coated sensor: biotinylated sequence for padlock immobilization - complementary sequence (biotin/20T/BS-, black) and non-complementary sequence (biotin/20T/BS+, red); heat-denatured padlock in ligation buffer and subsequent RCA for 1 hour.

Figure 26 shows the reflectivity curves $R(\theta)$ after padlock hybridization and pursuing RCA, respectively. Only in the case of hybridizing the padlock to its complementary primer (BS-) sequence a shift in the resonance angle was observed. By fitting this shift a considerable change in surface mass density of Γ_{RCA} = 14 ng/mm² was obtained. Additionally, the generation of ssDNA strands was confirmed by C2CA+/Cy5 labeling and showed a change of fluorescence intensity of $\Delta F_{PSP} > 10^5$ cps.

Evaluation of the experiment performed with an immobilized control sequence (BS+) whether showed a shift in the resonance angle nor an increase in fluorescence intensity and is in accordance with the previous described observations.

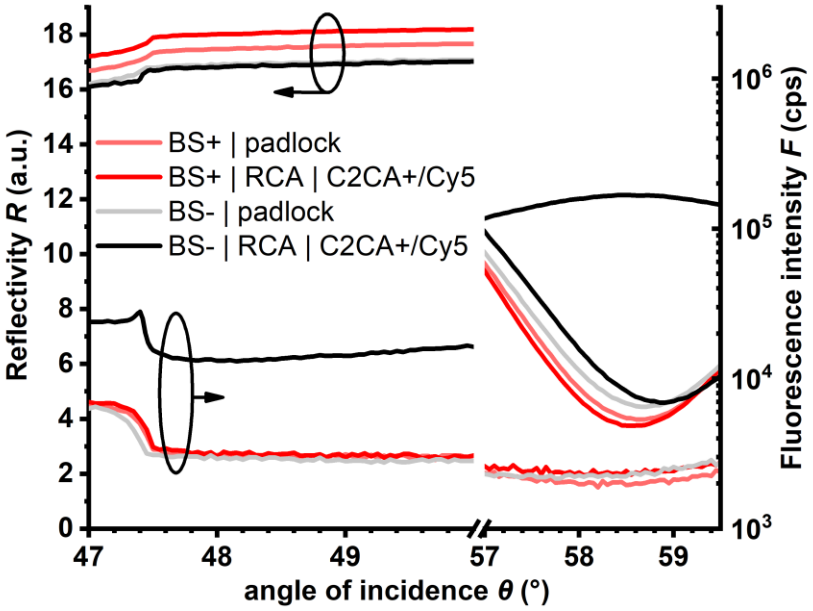

Figure 26: R(θ) after padlock immobilization and 1 hour of RCA followed by C2CA+/Cy5 labeling, respectively

6.3.3. Influence of ionic strength on brush conformation

Recent studies have shown that the DNA brush structure is highly dependent on its surrounding ion environment.[159] Many publications deal with properties and behaviour of surface-tethered DNA molecules to optimize the performance in microarray applications[160] and show that different aqueous environments cause changes in internucleotide distances[161], which as a consequence also strongly affects the grafting densities[162,163] and hybridization regimes of DNA microarrays.[164,165]

Figure 27 shows a schematic of the effect of increasing ionic strength on DNA brushes, which leads to the collapse of the DNA network.

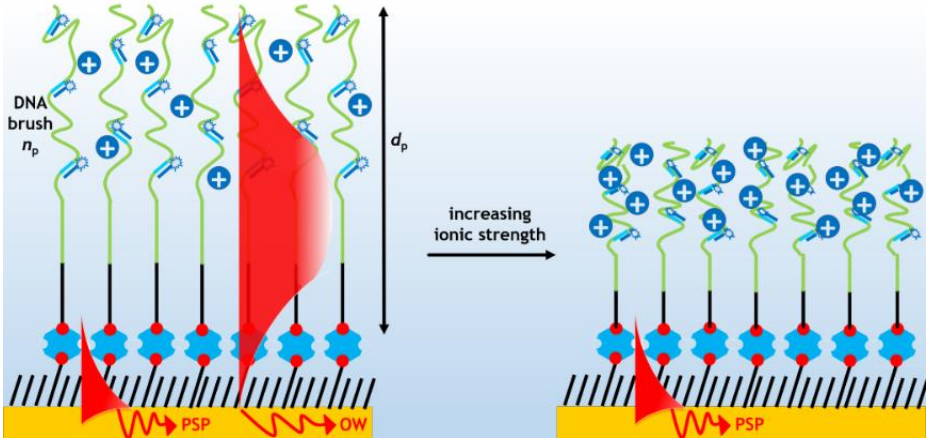

Figure 27: Effect of increasing ionic strength on surface tethered ssDNA strands.

To generate surface tethered ssDNA strands, a biotin/20T/TS-|padlock duplex, (see Ligation without exonuclease treatment) was bound to a neutravidin coated sensor chip. Since the RCA signal did not reach a plateau within the first hours of reaction, the solution containing ϕ29-Pol and dNTPs was flowed over the chip overnight (16.5 h) before the generated ssDNA strands were labeled with C2CA+/Cy5. The characteristics of the generated biointerface were obtained by analysing $R(\theta)$ curves (not shown) after each assay step and are summarized in Table 5.

Table 5: Characteristics of the generated biointerface containing ssDNA brushes in PBST buffer (n = 1.333).

	d **(nm)**	***n*** **(RIU)**	***Γ*** **(ng/mm²)**	***σ*** **(10^{-5} nmol/mm²)**
neutravidin	2.15	1.45	1.3	1.9
biotin/20T/TS- | padlock	0.85	1.45	0.5	1.2
RCA (16.5h)	2100	1.3366	28.4	

Figure 28 shows the recorded reflectivity spectrum $R(\theta)$ after RCA and C2CA+/Cy5 labeling. To study the effect of ionic strength on the DNA brush thickness, the ssDNA brushes were exposed to different concentrations (100 mM or 1 M) of monovalent (NaCl, KCl) and divalent ($MgCl_2$, $CaCl_2$) salts.

In PBST buffer the fluorescence intensity probed by the PSP mode was $F_{PSP} = 9.4 \cdot 10^4$ cps whereas the sharp dip in the fluorescence signal close to the critical angle was sufficiently higher $F_{TM1} = 1.6 \cdot 10^5$ cps. This observation confirmed that the Cy5 molecules could be excited by optical waveguides which travelled through the 2 µm thick ssDNA network.

However, with increasing salt concentration the fluorescence intensities probed by PSPs in the close vicinity of the metal surface increased. This together with the decreasing fluorescence intensities probed by the optical waveguide mode, indicates that the fluorophore labeled DNA strands got compacted. The right shift of the reflectivity curves to higher angles is explained by different refractive index of the solutions. At this point it should be noted that emission spectrum of fluorophores is also highly dependent on the solvent in which it is dissolved. Furthermore, the fluorescence intensities gradually decrease with time, when the excitation field is switched on which leads to bleaching of fluorescent dyes.

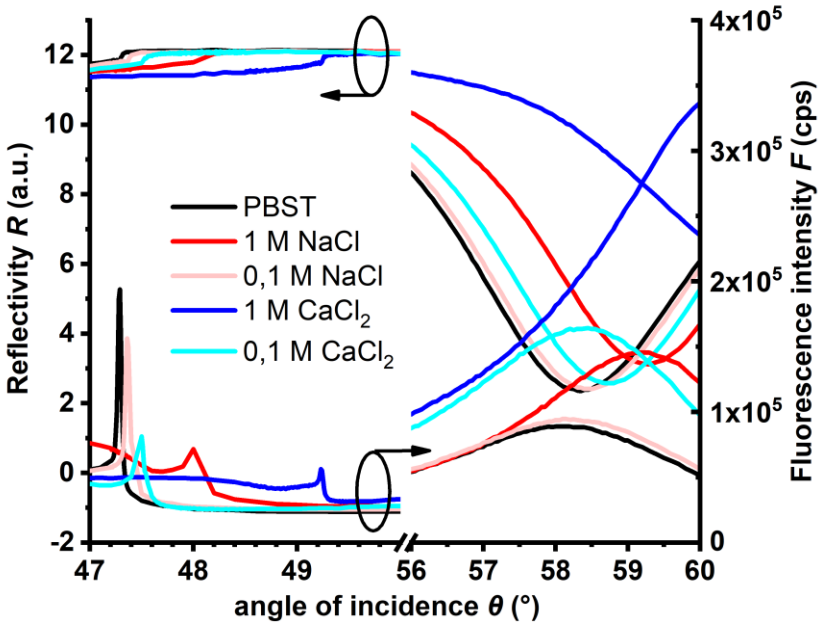

Figure 28: R(θ) of fluorophore labeled ssDNA brushes in the presence of different molar concentrations of monovalent (NaCl) and divalent ($CaCl_2$) salt solutions.

This feature of collapsing the DNA network (depicted in Figure 27), hence bringing the fluorophores closer to the evanescent field, increases the measured fluorescence intensity by a factor of ~3.5.

The influence of DNA brush thickness and its corresponding refractive index profile was determined by fitting the reflectivity spectrum $R(\theta)$ in different ionic solutions (c.f. Figure 28). The refractive index of the aqueous solution was determined individually on a bare gold chip. Figure 29 shows the fitted thickness and the refractive index of the surface-bound DNA strands. The decrease in brush height d_{RCA} is accompanied by compaction of the brush network, manifested as an increase in refractive index n_{RCA}. The thickness of the DNA brushes was decreased by a factor of 10, by changing the aqueous ion environment of surface-bound DNA strands from KCl to $CaCl_2$ at a molar concentration of 100 mM respectively.

Additionally the DNA brush thickness showed comparable values in the presence of monovalent ions at a molar concentration of 1 M as well as in the case of 100 mM $MgCl_2$

This indicates that divalent cations screen the two negative charges per ssDNA nucleotide more effective than monovalent counterions.

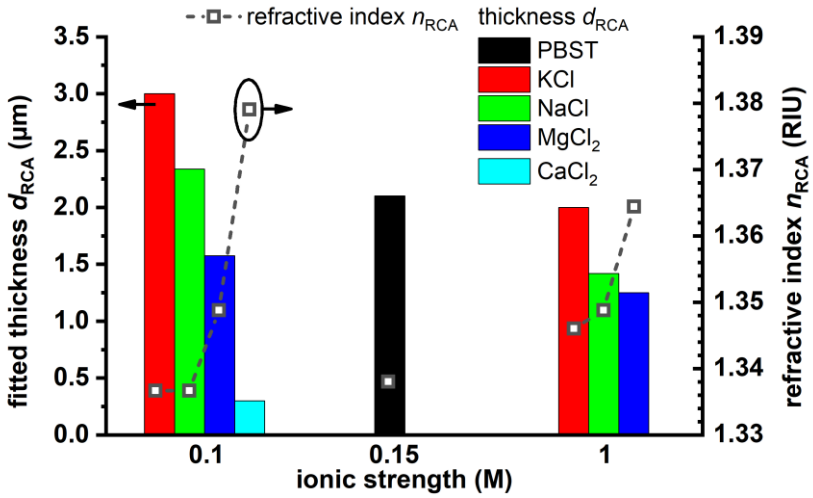

Figure 29: Thickness d_{RCA} (bar chart) and refractive index n_{RCA} profile (point-line) of ssDNA brush in different ionic environments (refractive index of the electrolytes; 150 mM PBST = 1.333, 100 mM: NaCl/KCl = 1.332, $MgCl_2$/$CaCl_2$ = 1.3342; 1 M: NaCl/KCl = 1.342, $MgCl_2$/$CaCl_2$ = 1.3527).

Similar observations have been reported by Petrovykh et al., who speculate that the negatively charged ssDNA backbone changes its molecular conformation and gets compacted through electrostatic crosslinking in buffers containing Ca^{2+} and Mg^{2+}.[166]

6.3.4. Amplification speed

To determine the amplification speed and hence the ultimate thickness of the surface-initiated growth of ssDNA strands, a plasmonic biosensor was saturated with neutravidin (σ_{NA} = 2.6·10^{-5} nmol/mm²). The padlock circularization through ligation was conducted in the presence of biotin/20T/TS- primer (see Ligation without exonuclease treatment) for 3 hours to increase the ligation efficiency. It should be noted, that the flow cell volume was reduced from 25 to 10 µL, by using another PDMS gasket with a thickness of 130 µm in all following experiments.

Continuously recorded angular reflectivity scans (see Figure 30) allowed to track the elongation process of immobilized padlock sequence ($\sigma_{biotin/20T/TS-|padlock}$ = 1.8·10^{-5} nmol/mm²) in-situ over time.

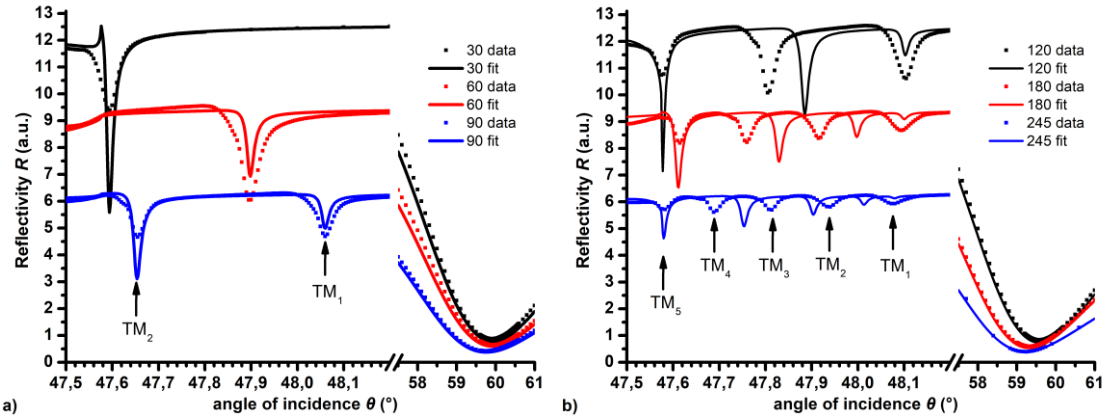

Figure 30: R(θ) at different time points after RCA initiation (t = 0 min), the solid lines present the curves fitted by Fresnel reflectivity model to the recorded data points shown as dots. a) at t = 30, 60 and 90 minutes b) at t = 120, 180 and 245 minutes.

The resonant excitation of up to five additional optical waveguide modes (see TM_1 – TM_5 in Figure 30b), allowed to follow the RCA reaction process every 15 minutes. The reflectivity curves $R(\theta)$ were fitted in a way that the combination of the refractive index n_{RCA} and the thickness d_{RCA} of the RCA product matched the first and the last resonant dip in the angular range θ = 47.5 – 48.2°. Until a RCA reaction time of 1 hour only one optical mode (TM_1) was excited which did not allow to independently determine the thickness and the refractive index of the DNA polymer layer, therefore the refractive index was kept constant and only the thickness of the RCA product was determined. The

obtained values for the thickness and refractive index at each given time point are plotted in Figure 31.

Strikingly, the gradual incorporation of nucleotides by ϕ29-DNA-polymerase generated a polymer layer with a thickness of d_{RCA} = 11.2 µm within 4 hours of RCA. The accumulated surface mass density (Γ_{RCA} = 354 ng/mm²) after 4 hours of RCA corresponds to 60 kb or 740 copies per immobilized strand. The number of calculated nucleotides was plotted as a function over time (red curve in Figure 31) and can be seen as the rate of DNA amplification through ϕ29-Pol per immobilized padlock. The curve shows a linear regime with an average speed of 280 nt/min. This value is lower than the minimum amplification rate of 330 nt/min obtained by RCA in the liquid phase at room temperature (see 6.2) and indicates that the RCA reaction is less efficient, when performed on a solid support. Comparing the average extension rates of common thermostable DNA polymerases with a speed of ~2400 nt/min at 75°C[167] to the obtained one shows that ϕ29-polymerase incorporated nucleotides with a 9-times lower speed.

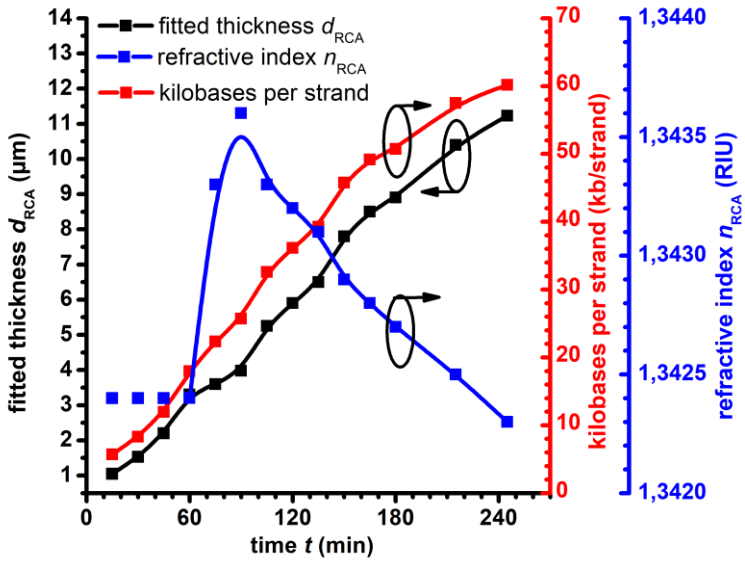

Figure 31: Thickness d_{RCA} and refractive index n_{RCA} profile of the generated ssDNA brush and the corresponding number of kiliobases per immobilized padlock as a function of RCA duration in an aqueous environment with n = 1.336(4h).

Interestingly the refractive index n_{RCA} of the generated ssDNA brushes increased in the RCA reaction time from 60 to 90 minutes, before it started to continuously drop down to lower values. This trend in the data allows to speculate about changes in the conformation of the surface-tethered ssDNA strands and might indicate that the ssDNA

strands altered their conformation from a mushroom to a more brush-like structure. A possible explanation could be that not every immobilized biotin/20T/TS-|padlock duplex got elongated at the same time and the sparsely packed chains took on a mushroom conformation. However, within the RCA process more and more strands get elongated and due to the electrostatic repulsion of DNA strands the oligonucleotide strands stretched away from the substrate to form a brush.

Previous results on the chain segment distribution ρ as a function of distance from the substrate in good solvents revealed comparable results, showing that the maximum chain segment distribution of tethered DNA strands is reached at a distance far away from the surface.[168,169] They found that the chain segment distribution falls off normal if the radius of gyration (R_g) equals the distance of the end-tethered DNA strand to the surface (see Figure 32). The refractive index n_{RCA} of the RCA product can be seen as the segment distribution ρ of the polymer chain, composed of N segments. The data showed that 25 kb ssDNA strands with a thickness of d_{RCA} = 4 µm exhibit a maximum ρ, which is manifested as a peak in n_{RCA} = 1.3436 at t_{RCA} = 90 minutes of reaction.

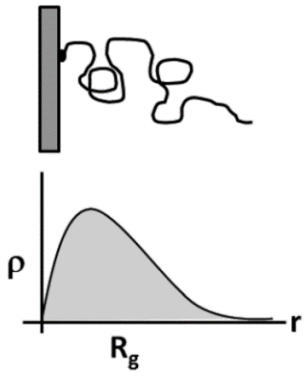

Figure 32: Schematic of surface-tethered DNA and its chain segment distribution ρ as a function of distance r from the surface (reprinted from [160]).

6.4. Control of chain growth

Previous experiments showed that surface tethered ssDNA strands protrude out of the evanescent field and supported the guidance of various waveguide modes by forming high-density brushes. However, a plasmonic sensor is the most sensitive within the exponentially decaying field probed by PSPs. To prevent that the long DNA strand stretches out of the confined field of PSPs, the ssDNA strand was tethered to the sensor surface by introducing an oligonucleotide strand which is complementary to the RCA product.

In particular, the biotinylated tether sequence (biotin/20T/TS+) was composed of a 20-nucleotide thymine spacer and the reverse complementary sequence of the target sequence. The 3' end was modified with a dideoxycytidine (ddC) which prevents the extension by the used polymerase which would lead to the double-strand formation of the RCA product and hence hinder Cy5 labelling.

The padlock probe was ligated for 2 hours in the presence of the target sequence (Figure 33). To study to the effect of padlock concentration on the RCA, the concentration of TS- was 8 and 80 nM, respectively. It can be assumed that a 10 times lower target concentration leads to 10 times lower concentration of circular padlock. Unreacted linear DNA was removed by exonuclease I as stated in the methods section "Ligation with exonuclease (Exo I) treatment" before the circular padlock was hybridized to its biotinylated complementary primer sequence (biotin/20T/BS-).

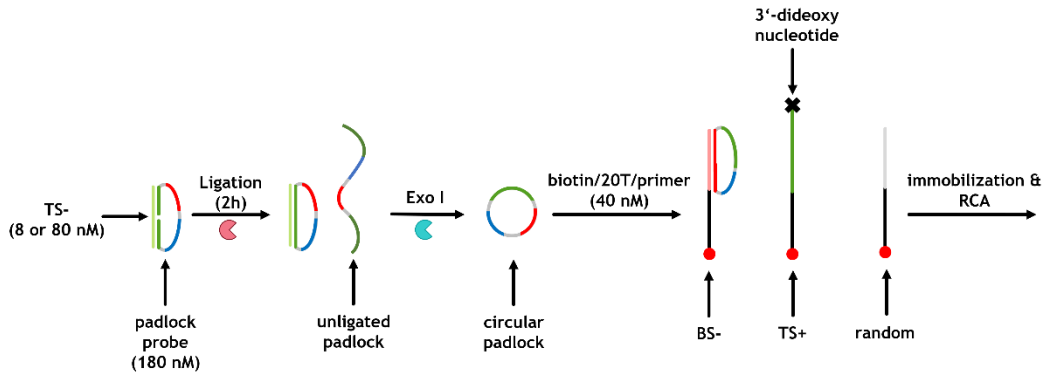

Figure 33: Padlock circularization through ligation followed by Exonuclease I (Exo I) treatment and padlock hybridization to its corresponding primer sequence (biotin/20T/BS-, rose); the tether sequence (biotin/20T/TS+, green) contains a dideoxynucleotide (ddC) to prevent its 3'-extension by the polymerase; an oligonucleotide containing a randomized sequence (biotin/20T/random).

This step was performed ex-situ to ensure padlock hybridization in order to form a biotin/20T/BS-|padlock duplex and to allow its immobilization on the neutravidin layer. After immobilization of the biotinylated oligonucleotides, RCA was conducted for 100 minutes.

To investigate, if tethering the ssDNA strands can enhance the sensitivity of the pursued assay, a comparative study of RCA on different surface architectures has been performed (see Figure 34).

(A)	brush	contains circular padlocks immobilized via the biotinylated primer sequence (biotin/20T/BS-); the RCA product forms brushes which protrude out of the evanescent field if a high concentration of the padlock is immobilized
(B)	tethering	contains a mixture of the primer sequence (biotin/20T/BS-) and the tether sequence (biotin/20T/TS+) at a ratio of 4:1 to bind the RCA product to the sensor surface
(C)	control	the tether sequence was replaced by a non-complementary randomized sequence (biotin/20T/random)

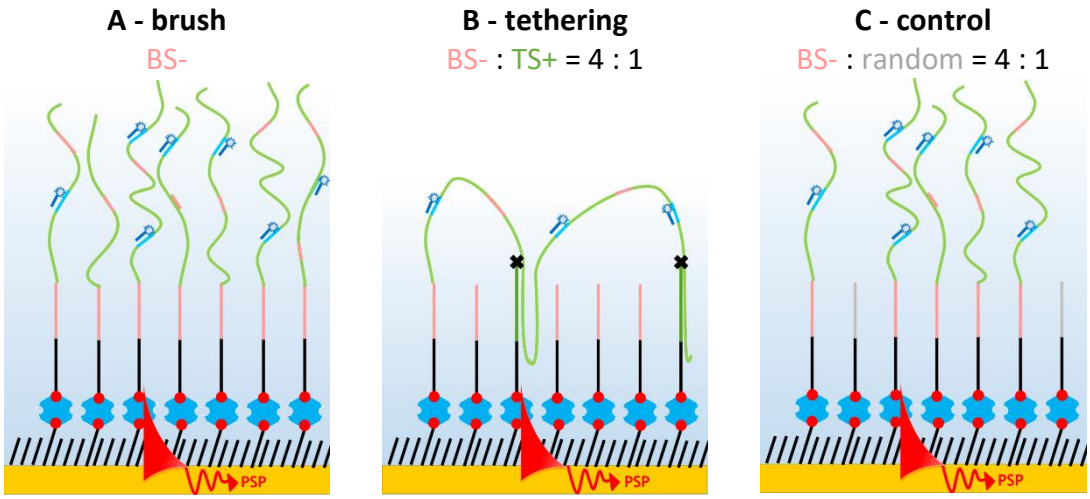

Figure 34: Schemes of different surface architectures on a plasmonic biosensor after RCA. (A) RCA on biointerface containing only the primer sequence (BS-, rose) (B) Tethering of RCA product on a surface containing a 4:1 mixture of BS- primer and TS+ respectively (green) (C) biointerface containing a 4:1 mixture of BS- primer and a non-complementary randomized (grey) control oligonucleotide

Figure 35a shows the angular reflectivity spectra $R(\theta)$ after RCA and Cy5 labeling on the different surface architectures in the case of high padlock concentration. It shows that RCA could generate thick DNA polymer brushes ($d_{RCA(A)}$ = 7.5 µm, $\Gamma_{RCA(A)}$ = 235 ng/mm²) on biointerface A, which is manifested as four sharp resonant dips in the reflectivity spectrum. In contrast to that, the absence of those resonant dips close to the

critical angle confirmed that the ssDNA strand was tethered to the surface in the case of biointerface B. To confirm this finding, the tether sequence was replaced by a randomized oligonucleotide (biointerface C). Evaluation of the reflectivity spectrum revealed a brush thickness of $d_{RCA(B)}$ = 5.0 µm with a surface mass density of $\Gamma_{RCA(B)}$ = 130 ng/mm² and verified the specificity of the RCA product to its tether sequence.

However, in the tethered approach, the shift in the resonance angle was unexpectedly low. The obtained mass surface density ($\Gamma_{RCA(C)}$ = 0.4 ng/mm²) was ~300-600 times lower in comparison to the biointerface A and C (see Figure 36). At this point, it is worth mentioning, that affinity binding of the padlock in the BS-|TS+ mixture to the neutravidin layer led to a considerably lower sensor response. For this observation, no possible explanation was found and further experiments would be needed.

To compare the obtained results, the padlock concentration was reduced by a ten-fold. This was achieved by performing the ligation reaction in the presence of a lower concentration of target sequence (8 nM TS-). All $R(\theta)$ curves in Figure 35b lack the resonant features in the angular regime of θ = 47-49 °. This revealed that at a lower concentration of circular padlock, the ssDNA strands could not stretch into the evanescent field and proved that ssDNA strands behave similar as immobilized polyelectrolyte brushes on solid supports. At lower grafting densities of surface-tethered ssDNA strands could not form a brush-like surface architecture, but instead took on a mushroom-like conformation.

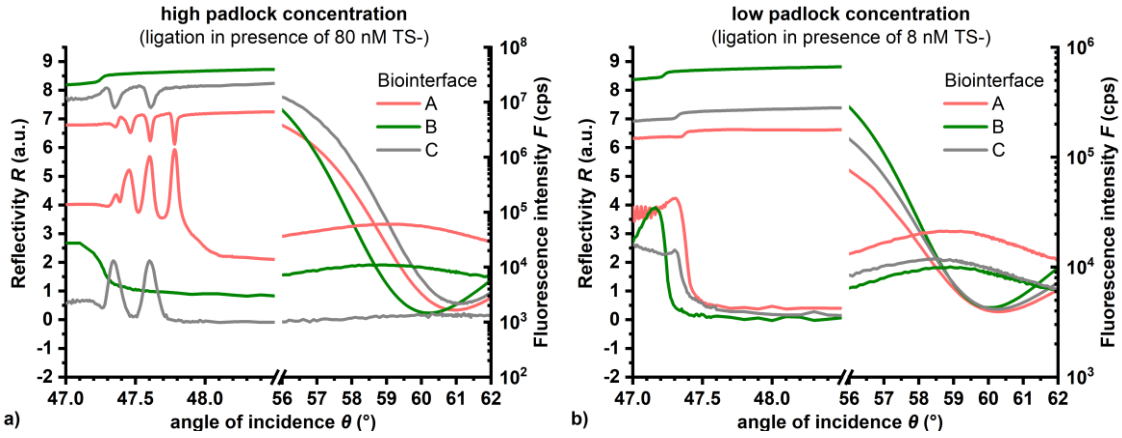

Figure 35: R(θ) of plasmonic biosensor after RCA and fluorophore labeling a) high circular padlock concentration b) low circular padlock concentration.

Figure 36 shows a summary of surface mass densities revealed after each immobilization step. SPR-detection principle allowed to immobilize neutravidin with constant surface mass densities of Γ = 2.15 ± 0.13 ng/mm² on six individual chips. As already mentioned beforehand, the padlock mixture containing the universal barcode sequence (biotin/20T/BS-) and the tether sequence (biotin/20T/TS+) in the tether approach led to lower mass surface densities than in the mixtures containing the biotin/20T/BS- or the biotin/20T/random control sequence.

In all cases, RCA increased the sensor response, manifested as increase in surface mass densities as well as fluorescence intensities. In the case of biointerface A and C, the sensor responses scaled with the amount of padlock concentration. However, it seems that RCA was inhibited in the tether approach. A possible explanation for this could be steric hindrance of the Polymerase which cannot elongate the surface bound strand further.

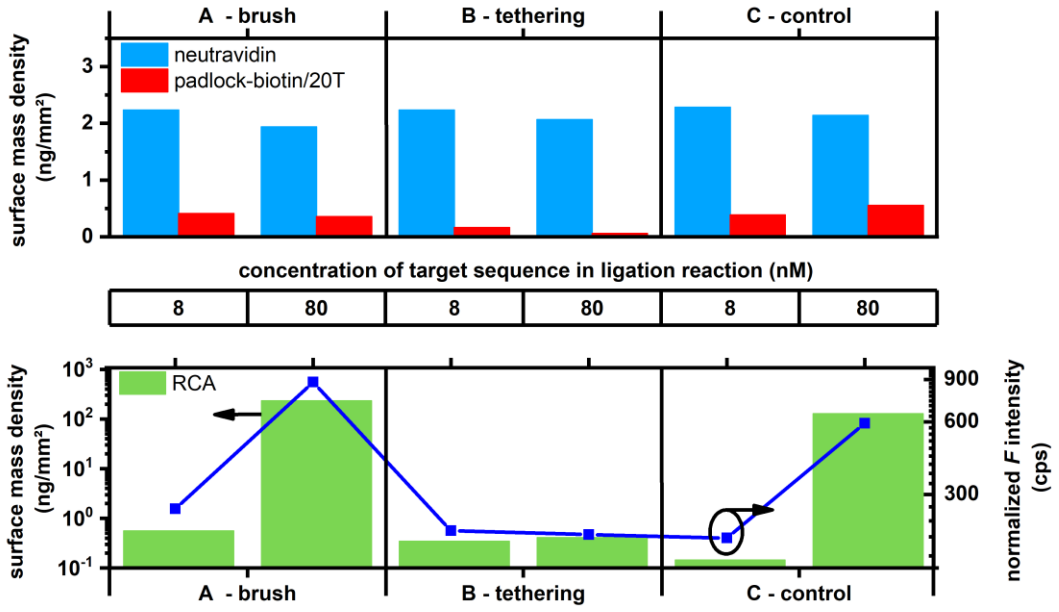

Figure 36: Surface mass densities after each immobilization step on three different surface architectures (A-C); the circular padlock probes were obtained through ligation reactions containing either 80 or 8 nM of TS-.The normalized fluorescence intensities were extracted from the R(t) measurements (data not shown) after 10 minutes of Cy5 labeling followed by PBST rinsing for 5 minutes; the intensities were normalized to the fluorescence sensor response of Cy5-labeled oligonucleotides at different molar concentrations prior to RCA.

7. Summary and outlook

This thesis demonstrates the detection of an antibiotic resistance gene of bacterial species through ligation-mediated padlock circularization and subsequent isothermal DNA amplification through RCA on a metallic thin film.

The feasibility of the assay concept was firstly shown in the liquid phase. The oligonucleotides and the RCA product were characterized by standard agarose gel electrophoresis. The determined extension rate of ϕ29-Polymerase in the liquid phase was 330 nt/min at room temperature.

As a next step the assay was implemented on a plasmonic biosensor with a controlled biointerface. SPR and SPFS detection principle allowed the highly specific and sensitive detection of the surface-initiated growth of ssDNA strands. The specificity of fluorophore labeling of the generated RCA product showed a 130-fold higher sensor response when introducing its complementary fluorophore modified oligonucleotide in comparison to a non-complementary, randomized oligonucleotide. Furthermore, it was shown that RCA can only be conducted if the circularized padlock probe is immobilized to the sensor surface via its complementary primer sequence.

The properties and behaviour of the generated ssDNA brushes in the presence of different aqueous environments demonstrated that surface-tethered DNA strands behave similar to polyelectrolyte brushes and therefore can be compacted by increasing the ionic strength and by the usage of divalent salts.

Furthermore, the speed of DNA strand prolongation was determined by optical waveguide spectroscopy in situ over time. The extension rate of the polymerase was 280 nt/min and lead to surface-bound DNA brushes with an end-to end distance of 11 µm. This difference in speed is caused by the surface bound amplification method which leads to steric hindrance in the elongation process.

A strategy to prevent that the long DNA strands protrude out of the exponentially decaying field probed by PSPs is proposed. This includes the implementation of an oligonucleotide sequence to tether the RCA product to the sensor surface. In order to

evaluate this concept and potentially increase the sensitivity with the proposed strategy, more experiments have to be performed.

However, it is demonstrated that isothermal enzymatic DNA amplification via RCA provide means to generate long surface bound ssDNA strands which can be detected and characterised by SPR, OWS and SPFS detection principle. To the author's knowledge, this is the first report of following the process of DNA polymer brush synthesis in-situ on a solid support. The results provide insight in the process of DNA elongation and the change in chain conformation in dependency of the grafting density of the circular padlock probe.

The results and the proposed assay concept will be translated to several target DNA sequences which allows the detection of several antibiotic resistance genes in a multiplexed format. For this, a digital readout platform will be employed to detect the individual RCA products on microarrays.

8. References

1. World Health Organization (WHO). Antibiotic resistance. Website. https://www.who.int/news-room/fact-sheets/detail/antibiotic-resistance. Published 2018. Accessed April 7, 2020.
2. World Health Organization (WHO). Antimicrobial resistance. Website. https://www.who.int/news-room/fact-sheets/detail/antimicrobial-resistance. Published 2018. Accessed April 7, 2020.
3. O'Neill J. Antimicrobial Resistance: Tackling a Crisis for the Health and Wealth of Nations. *Rev Antimicrob Resist*. 2014. https://amr-review.org/sites/default/files/AMR Review Paper - Tackling a crisis for the health and wealth of nations_1.pdf.
4. O'Neill J. Tackling drug-resistant infections globally: Final report and recommendations. *Rev Antimicrob Resist*. 2016. https://amr-review.org/sites/default/files/160518_Final paper_with cover.pdf.
5. Centers for Disease Control and Prevention (CDC). Antibiotic / Antimicrobial Resistance (AR/AMR). Website. https://www.cdc.gov/drugresistance/about.html. Published 2020. Accessed April 7, 2020.
6. Fleming A. On the Antibacterial Action of Cultures of a Penicillium, with Special Reference to their Use in the Isolation of B. influenzæ. *Br J Exp Pathol*. 1929;10(3):226-236.
7. Abraham EP, Chain E. An Enzyme from Bacteria able to Destroy Penicillin. *Nature*. 1940;146:837. doi:10.1038/146837a0
8. Rossolini GM, Arena F, Giani T. Mechanisms of Antibacterial Resistance. In: Cohen J, Powderly WG, Opal SM, eds. *Infectious Diseases*. 4th ed. Elsevier Ltd.; 2017:1181-1196. doi:10.1016/B978-0-7020-6285-8.00138-6
9. Bush K. Proliferation and significance of clinically relevant β-lactamases. *Ann N Y Acad Sci*. 2013;1277(1):84-90. doi:10.1111/nyas.12023
10. Bush K, Bradford PA. β-Lactams and β-Lactamase Inhibitors: An Overview. *Cold Spring Harb Perspect Med*. 2016;6(8):a025247. doi:10.1101/cshperspect.a025247
11. Baker SJ, Payne DJ, Rappuoli R, De Gregorio E. Technologies to address antimicrobial resistance. *Proc Natl Acad Sci U S A*. 2018;115(51):12887-12895. doi:10.1073/pnas.1717160115
12. Walther-Rasmussen J, Høiby N. OXA-type carbapenemases. *J Antimicrob Chemother*. 2006;57(3):373-383. doi:10.1093/jac/dki482
13. Nordmann P, Dortet L, Poirel L. Carbapenem resistance in Enterobacteriaceae : here is the storm ! *Trends Mol Med*. 2012;18(5):263-272. doi:10.1016/j.molmed.2012.03.003
14. Mathers A, Hazen KC, Carroll J, et al. First Clinical Cases of OXA-48-Producing Carbapenem-Resistant Klebsiella pneumoniae in the United States: the "Menace" Arrives in the New World. *J Clin Microbiol*. 2013;51(2):680-683. doi:10.1128/JCM.02580-12
15. van Hoek AHAM, Mevius D, Guerra B, Mullany P, Roberts AP, Aarts HJM. Acquired antibiotic resistance genes: an overview. *Front Microbiol*. 2011;2(203):1-27. doi:10.3389/fmicb.2011.00203
16. Butaye P, Argudín MÁ, Threlfall J. Introduction to Antimicrobial-Resistant Foodborne Pathogens. In: Chen C-Y, Yan X, Jackson CR, eds. *Antimicrobial Resistance and Food Safety: Methods and Techniques*. 1st ed. London, San Diego, Waltham, Oxford: Elsevier Inc.; 2015:1-17. doi:10.1016/B978-0-12-801214-7.00001-6
17. Kadlec K, Wendlandt S, Feßler AT, Schwarz S. Methods for the Detection of Antimicrobial Resistance and the Characterization of Staphylococcus aureus Isolates from Food-Producing Animals and Food of Animal Origin. In: Chen C-Y, Yan X, Jackson CR, eds. *Antimicrobial Resistance and Food Safety: Methods and Techniques*. 1st ed. London, San Diego, Waltham, Oxford: Elsevier Inc.; 2015:207-232. doi:10.1016/B978-0-12-801214-7.00011-9
18. Schubert S, Heesemann J. Pathogenomics: Application and New Diagnostic Tools. In: Hacker J,

Dobrindt U, eds. *Pathogenomics: Genome Analysis of Pathogenic Microbes*. Weinheim: WILEY-VCH Verlag GmbH & Co. KGaA; 2006:481-504. doi:10.1002/352760801X.ch22

19. Anjum MF, Zankari E, Hasman H. Molecular Methods for Detection of Antimicrobial Resistance. *Microbiol Spectr*. 2017;5(6):1-17. doi:10.1128/microbiolspec.arba-0011-2017
20. Jorgensen JH, Ferraro MJ. Antimicrobial Susceptibility Testing: A Review of General Principles and Contemporary Practices. *Clin Infect Dis*. 2009;49(11):1749-1755. doi:10.1086/647952
21. Khan ZA, Siddiqui MF, Park S. Current and Emerging Methods of Antibiotic Susceptibility Testing. *Diagnostics (Basel)*. 2019;9(2):49. doi:10.3390/diagnostics9020049
22. Syal K, Mo M, Yu H, et al. Current and emerging techniques for antibiotic susceptibility tests. *Theranostics*. 2017;7(7):1795-1805. doi:10.7150/thno.19217
23. Puttaswamy S, Gupta SK, Regunath H, Smith LP, Sengupta S. A Comprehensive Review of the Present and Future Antibiotic Susceptibility Testing (AST) Systems. *Arch Clin Microbiol*. 2018;09(3):1-9. doi:10.4172/1989-8436.100083
24. Llor C, Bjerrum L. Antimicrobial resistance : risk associated with antibiotic overuse and initiatives to reduce the problem. *Ther Adv Drug Saf Rev*. 2014;5(6):229-241. doi:10.1177/2042098614554919
25. Cockerill Iii FR. Genetic Methods for Assessing Antimicrobial Resistance. *Antimicrob Agents Chemother*. 1999;43(2):199-212.
26. Caetano-Anollés D. *Polymerase Chain Reaction*. Vol 5. 2nd ed. Elsevier Inc.; 2013. doi:10.1016/B978-0-12-374984-0.01186-4
27. Applied Biological Materials. Polymerase Chain Reaction (PCR) - An Introduction. Website. https://old.abmgood.com/marketing/knowledge_base/polymerase_chain_reaction_introduction.php. Accessed April 20, 2020.
28. Doyle D, Peirano G, Lascols C, Lloyd T, Church DL, Pitouta JDD. Laboratory detection of Enterobacteriaceae that produce carbapenemases. *J Clin Microbiol*. 2012;50(12):3877-3880. doi:10.1128/JCM.02117-12
29. Morrison TB, Weis JJ, Wittwer CT. Quantification of lowcopy transcripts by continuous SYBR® green I monitoring during amplification. *Biotechniques*. 1998;24(6):954-962.
30. Heid CA, Stevens J, Livak K, Williams PM. Real time quantitative PCR. *Genome Res*. 1996;6:986-994. doi:10.1101/gr.6.10.986
31. Seifi M, Ghasemi A, Heidarzadeh S, et al. Overview of Real-Time PCR Principles. In: *Polymerase Chain Reaction*. ; 2012:405-442. doi:10.5772/39220
32. Arya M, Shergill IS, Williamson M, Gommersall L, Arya N, Patel HRH. Basic principles of real-time quantitative PCR. *Expert Rev Mol Diagn*. 2005;5(2):209-219. doi:10.1586/14737159.5.2.209
33. Wittwer CT, Herrmann MG, Gundry CN, Elenitoba-Johnson KSJ. Real-time multiplex PCR assays. *Methods*. 2001;25(4):430-442. doi:10.1006/meth.2001.1265
34. Behzadi P. DNA microarrays and multidrug resistant bacteria. *Eur Pharm Rev*. 2018;23(1):30-32.
35. Rajagopal A, Yurk D, Shin C, et al. Significant Expansion of Real-Time PCR Multiplexing with Traditional Chemistries using Amplitude Modulation. *Sci Rep*. 2019;9(1):1-8. doi:10.1038/s41598-018-37732-y
36. Letsinger RL, Mahadevan V. Oligonucleotide Synthesis on a Polymer Support1,2. *J Am Chem Soc*. 1965;87(15):3526-3527. doi:10.1021/ja01093a058
37. Grunstein M, Hogness DS. Colony hybridization: A method for the isolation of cloned DNAs that contain a specific gene. *Proc Natl Acad Sci*. 1975;72(10):3961-3965.
38. Bumgarner R. DNA microarrays: Types, Applications and their future Roger. *Curr Protoc Mol Biol*. 2013;Chapter 22(Unit 22.1). doi:10.1002/0471142727.mb2201s101
39. DeRisi J, Penland L, Brown PO, et al. Use of a cDNA microarray to analyse gene expression patterns in human cancer. *Nat Genet*. 1996;14(4):457-460. doi:10.1038/ng1296-457
40. Southern E. DNA Microarrays: History and Overview. Rampal JB, ed. *Methods Mol Biol*.

2001;170(1-15). doi:10.1385/1-59259-234-1:1

41. Card R, Zhang J, Das P, Cook C, Woodford N, Anjum MF. Evaluation of an expanded microarray for detecting antibiotic resistance genes in a broad range of gram-negative bacterial pathogens. *Antimicrob Agents Chemother*. 2013;57(1):458-465. doi:10.1128/AAC.01223-12

42. Dally S, Lemuth K, Kaase M, Rupp S, Knabbe C, Weile J. DNA microarray for genotyping antibiotic resistance determinants in acinetobacter baumannii clinical isolates. *Antimicrob Agents Chemother*. 2013;57(10):4761-4768. doi:10.1128/AAC.00863-13

43. Frye JG, Lindsey RL, Rondeau G, et al. Development of a DNA microarray to detect antimicrobial resistance genes identified in the national center for biotechnology information database. *Microb Drug Resist*. 2010;16(1):9-19. doi:10.1089/mdr.2009.0082

44. Perreten V, Vorlet-Fawer L, Slickers P, Ehricht R, Kuhnert P, Frey J. Microarray-based detection of 90 antibiotic resistance genes of gram-positive bacteria. *J Clin Microbiol*. 2005;43(5):2291-2302. doi:10.1128/JCM.43.5.2291-2302.2005

45. Wellinghausen N, Kochem AJ, Disqué C, et al. Diagnosis of bacteremia in whole-blood samples by use of a commercial universal 16S rRNA gene-based PCR and sequence analysis. *J Clin Microbiol*. 2009;47(9):2759-2765. doi:10.1128/JCM.00567-09

46. Huang RSP, Johnson CL, Pritchard L, Hepler R, Ton TT, Dunn JJ. Performance of the Verigene® enteric pathogens test, Biofire FilmArray™ gastrointestinal panel and Luminex xTAG® gastrointestinal pathogen panel for detection of common enteric pathogens. *Diagn Microbiol Infect Dis*. 2016;86(4):336-339. doi:10.1016/j.diagmicrobio.2016.09.013

47. Naas T, Cuzon G, Bogaerts P, Glupczynski Y, Nordmann P. Evaluation of a DNA microarray (check-MDR CT102) for rapid detection of TEM, SHV, and CTX-M extended-spectrum β-lactamases and of KPC, OXA-48, VIM, IMP, and NDM-1 carbapenemases. *J Clin Microbiol*. 2011;49(4):1608-1613. doi:10.1128/JCM.02607-10

48. Wolff N, Hendling M, Schönthaler S, Geiss AF, Barišić I. Low-cost microarray platform to detect antibiotic resistance genes. *Sens Bio-Sensing Res*. 2019;23(October 2018):100266. doi:10.1016/j.sbsr.2019.100266

49. Dai H, Meyer M, Stepaniants S, Ziman M, Stoughton R. Use of hybridization kinetics for differentiating specific from non-specific binding to oligonucleotide microarrays. *Nucleic Acids Res*. 2002;30(16):e86. doi:10.1093/nar/gnf085

50. Adessi C. Solid phase DNA amplification: characterisation of primer attachment and amplification mechanisms. *Nucleic Acids Res*. 2000;28(20):e87. doi:10.1093/nar/28.20.e87

51. Tjong V, Yu H, Hucknall A, Rangarajan S, Chilkoti A. Amplified on-chip fluorescence detection of DNA hybridization by surface-initiated enzymatic polymerization. *Anal Chem*. 2011;83(13):5153-5159. doi:10.1021/ac200946t

52. Ericsson O, Jarvius J, Schallmeiner E, et al. A dual-tag microarray platform for high-performance nucleic acid and protein analyses. *Nucleic Acids Res*. 2008;36(8). doi:10.1093/nar/gkn106

53. del Solar G, Giraldo R, Ruiz-Echevarría MJ, Espinosa M, Díaz-Orejas R. Replication and Control of Circular Bacterial Plasmids. *Microbiol Mol Biol Rev*. 1998;62(2):434-464. doi:10.1128/mmbr.62.2.434-464.1998

54. Kornberg A, Baker T. *DNA Replication*. New York: W H Freeman & Co; 1992.

55. Gilbert W, Dressler D. DNA replication: the rolling circle model. *Cold Spring Harb Symp Quant Biol*. 1968;33:473-484. doi:10.1101/sqb.1968.033.01.055

56. Goo NI, Kim DE. Rolling circle amplification as isothermal gene amplification in molecular diagnostics. *Biochip J*. 2016;10(4):262-271. doi:10.1007/s13206-016-0402-6

57. Fakruddin M, Mannan KS, Chowdhury A, et al. Nucleic acid amplification: Alternative methods of polymerase chain reaction. *J Pharm Bioallied Sci*. 2013;5(4):245-252. doi:10.4103/0975-7406.120066

58. Lau HY, Botella JR. Advanced DNA-based point-of-care diagnostic methods for plant diseases detection. *Front Plant Sci*. 2017;8(December):1-14. doi:10.3389/fpls.2017.02016

59. Blanco L, Bernad A, Lazaro JM, Martin G, Garmendia C, Salas M. Highly efficient DNA synthesis by the phage Φ29 DNA polymerase. Symmetrical mode of DNA replication. *J Biol Chem*. 1989;264(15):8935-8940. doi:10.13039/100000002

60. Zhou C, Zou H, Sun C, Ren D, Chen J, Li Y. Signal amplification strategies for DNA-based surface plasmon resonance biosensors. *Biosens Bioelectron*. 2018;117(June):678-689. doi:10.1016/j.bios.2018.06.062

61. Gu L, Yan W, Liu L, Wang S, Zhang X, Lyu M. Research progress on rolling circle amplification (RCA)-based biomedical sensing. *Pharmaceuticals*. 2018;11(2):1-19. doi:10.3390/ph11020035

62. Ali MM, Li F, Zhang Z, et al. Rolling circle amplification: A versatile tool for chemical biology, materials science and medicine. *Chem Soc Rev*. 2014;43(10):3324-3341. doi:10.1039/c3cs60439j

63. Eriksson R, Jobs M, Ekstrand C, et al. Multiplex and quantifiable detection of nucleic acid from pathogenic fungi using padlock probes, generic real time PCR and specific suspension array readout. *J Microbiol Methods*. 2009;78(2):195-202. doi:10.1016/j.mimet.2009.05.016

64. Barišić I, Petzka J, Schoenthaler S, Vierlinger K, Noehammer C, Wiesinger-Mayr H. Multiplex characterization of human pathogens including species and antibiotic-resistance gene identification. *J Med Microbiol*. 2016;65(1):48-55. doi:10.1099/jmm.0.000192

65. Nilsson M, Malmgren H, Samiotaki M, Kwiatkowski M, Chowdhary BP, Landegren U. Padlock probes: Circularizing oligonucleotides for localized DNA detection. *Science (80-)*. 1994;265(5181):2085-2088. doi:10.1126/science.7522346

66. Barišić I, Kamleithner V, Schönthaler S, Wiesinger-Mayr H. Fast and highly specific DNA-based multiplex detection on a solid support. *Appl Microbiol Biotechnol*. 2014;99(1):413-423. doi:10.1007/s00253-014-6246-x

67. Russell C, Welch K, Jarvius J, et al. Gold nanowire based electrical DNA detection using rolling circle amplification. *ACS Nano*. 2014;8(2):1147-1153. doi:10.1021/nn4058825

68. Feng C, Mao X, Yang Y, Zhu X, Yin Y, Li G. Rolling circle amplification in electrochemical biosensor with biomedical applications. *J Electroanal Chem*. 2016;781:223-232. doi:10.1016/j.jelechem.2016.07.008

69. Linck L, Reiß E, Bier F, Resch-Genger U. Direct labeling rolling circle amplification as a straightforward signal amplification technique for biodetection formats. *Anal Methods*. 2012;4(5):1215-1220. doi:10.1039/c2ay05760c

70. Berr A, Schubert I. Direct labelling of BAC-DNA by rolling-circle amplification. *Plant J*. 2006;45(5):857-862. doi:10.1111/j.1365-313X.2005.02637.x

71. Kawamura A, Miyata T. Biosensors. In: *Biomaterials Nanoarchitectonics*. Elsevier Inc.; 2016:157-176. doi:10.1016/B978-0-323-37127-8/00010-8

72. Morales MA, Halpern JM. Guide to Selecting a Biorecognition Element for Biosensors. *Bioconjug Chem*. 2018;29(10):3231-3239. doi:10.1021/acs.bioconjchem.8b00592

73. Long F, Zhu A, Shi H. Recent advances in optical biosensors for environmental monitoring and early warning. *Sensors (Switzerland)*. 2013;13(10):13928-13948. doi:10.3390/s131013928

74. Rodriguez-Mozaz S, Lopez De Alda MJ, Barceló D. Biosensors as useful tools for environmental analysis and monitoring. *Anal Bioanal Chem*. 2006;386(4):1025-1041. doi:10.1007/s00216-006-0574-3

75. Malhotra BD, Pandey CM. *Biosensors : Fundamentals and Applications*. Shawbury, Shrewsbury, Shropshire, SY4 4NR, UK: Smithers Rapra Technology Ltd; 2017.

76. Helmerhorst E, Chandler DJ, Mamotte CD. Real-time and Label-free Bio-sensing of Molecular Interactions by Surface Plasmon Resonance: A Laboratory Medicine Perspective. *Clin Biochem Rev*. 2012;33:161-173.

77. Damborský P, Švitel J, Katrlík J. Optical biosensors. *Essays Biochem*. 2016;60(1):91-100. doi:10.1042/EBC20150010

78. Homola J. Surface plasmon resonance sensors for detection of chemical and biological species. *Chem Rev*. 2008;108(2):462-493. doi:10.1021/cr068107d

79. Liu J, Jalali M, Mahshid S, Wachsmann-Hogiu S. Are plasmonic optical biosensors ready for use in point-of-need applications? *Analyst*. 2020;145(2):364-384. doi:10.1039/c9an02149c

80. Fu Z, Lu Y-C, Lai JJ. Recent Advances in Biosensors for Nucleic Acid and Exosome Detection. *Chonnam Med J*. 2019;55(2):86-98. doi:10.4068/cmj.2019.55.2.86

81. Nguyen HH, Park J, Kang S, Kim M. Surface plasmon resonance: A versatile technique for biosensor applications. *Sensors (Switzerland)*. 2015;15(5):10481-10510. doi:10.3390/s150510481

82. Migliorini E, Weidenhaupt M, Picart C. Practical guide to characterize biomolecule adsorption on solid surfaces. *Biointerphases*. 2018;13(6):06D303. doi:10.1116/1.5045122

83. Peltomaa R, Glahn-Martínez B, Benito-Peña E, Moreno-Bondi MC. Optical Biosensors for Label-Free Detection of Small Molecules. *Sensors (Basel)*. 2018;18(12). doi:10.3390/s18124126

84. Tudos AJ, Schasfoort RBM. Introduction to surface plasmon resonance. In: Schasfoort RBM, Tudos AJ, eds. *Handbook of Surface Plasmon Resonance*. Cambridge, United Kingdom: Royal Society Of Chemistry; 2008:1-14. doi:10.1039/9781847558220-00001

85. Höppener C, Novotny L. Exploiting the light–metal interaction for biomolecular sensing and imaging. *Q Rev Biophys*. 2012;45(2):209-255. doi:10.1017/S0033583512000042

86. Lal S, Grady NK, Kundu J, Levin CS, Lassiter JB, Halas NJ. Tailoring plasmonic substrates for surface enhanced spectroscopies. *Chem Soc Rev*. 2008;37(5):898-911. doi:10.1039/b705969h

87. Lakowicz JR, Ray K, Chowdhury M, et al. Plasmon-controlled fluorescence: A new paradigm in fluorescence spectroscopy. *Analyst*. 2008;133(10):1308-1346. doi:10.1039/b802918k

88. Raether H. *Surface Plasmons on Smooth and Rough Surfaces and on Gratings*. Berlin: Springer-Verlag Berlin Heidelberg; 1988. doi:10.1007/BFb0048317

89. Homola J. *Surface Plasmon Resonance Based Sensors*. 4th ed. (Homola J, ed.). Springer Berlin Heidelberg; 2006.

90. Otto A. Excitation of nonradiative surface plasma waves in silver by the method of frustrated total reflection. *Zeitschrift für Phys*. 1968;216(4):398-410. doi:10.1007/BF01391532

91. Kretschmann E, Raether H. Radiative Decay of Non Radiative Surface Plasmons Excited by Light. *Zeitschrift fur Naturforsch - Sect A J Phys Sci*. 1968;23a(12):2135-2136. doi:10.1515/zna-1968-1247

92. Dostálek J, Knoll W. Biosensors based on surface plasmon-enhanced fluorescence spectroscopy (Review). *Biointerphases*. 2008;3(3):FD12-FD22. doi:10.1116/1.2994688

93. Lawrence CR, Geddes NJ, Furlong DN, Sambles JR. Surface plasmon resonance studies of immunoreactions utilizing disposable diffraction gratings. *Biosens Bioelectron*. 1996;11(4):389-400. doi:10.1016/0956-5663(96)82734-5

94. Homola J. Surface plasmon resonance sensors for detection of chemical and biological species. *Chem Rev*. 2008;108(2):462-493. doi:10.1021/cr068107d

95. Homola J, Yee SS, Gauglitz G. Surface plasmon resonance sensors: review. *Sensors Actuators, B Chem*. 1999;54(1):3-15. doi:10.1016/S0925-4005(98)00321-9

96. Dostálek J, Huang CJ, Knoll W. Tutorial Review: Surface Plasmon Resonance-Based Biosensors. In: Förch R, Schönherr H, Jenkins TA, eds. *Surface Design: Applications in Bioscience and Nanotechnology*. Wiley-VCH Verlag GmbH & Co. KGaA; 2009:29-53. doi:doi.org/10.1002/9783527628599.ch2

97. Dostálek J, Knoll W. Plasmonics. In: Matyjaszewski K, Möller M, eds. *Polymer Science: A Comprehensive Reference*. Vol 2. Amsterdam: Elsevier B.V.; 2012:647-659. doi:10.1016/B978-0-444-53349-4.00050-9

98. Liedberg B, Lundström I, Stenberg E. Principles of biosensing with an extended coupling matrix and surface plasmon resonance. *Sensors Actuators, B Chem*. 1993;11(1-3):63-72.

99. Lakowicz JR. *Principles of Fluorescence Spectroscopy*. 3rd ed. New York: Springer Science+Business Media; 2006. doi:10.1007/978-0-387-46312-4

100. Bauch M, Toma K, Toma M, Zhang Q, Dostalek J. Plasmon-Enhanced Fluorescence Biosensors: A

Review. *Plasmonics*. 2014;9(4):781-799. doi:10.1007/s11468-013-9660-5

101. Weber WH, Eagen CF. Energy transfer from an excited dye molecule to the surface plasmons of an adjacent metal. *Opt Lett*. 1979;4(8):236-238. doi:10.1364/ol.4.000236

102. Lakowicz JR. Radiative decay engineering 3. Surface plasmon-coupled directional emission. *Anal Biochem*. 2004;324(2):153-169. doi:10.1016/j.ab.2003.09.039

103. Liebermann T, Knoll W. Surface-plasmon field-enhanced fluorescence spectroscopy. *Colloids Surfaces A Physicochem Eng Asp*. 2000;171(1-3):115-130. doi:10.1016/S0927-7757(99)00550-6

104. Liebermann T, Knoll W. Parallel Multispot Detection of Target Hybridization to Surface-Bound Probe Oligonucleotides of Different Base Mismatch by Surface-Plasmon Field-Enhanced Fluorescence Microscopy. *Langmuir*. 2003;19(5):1567-1572. doi:10.1021/la026263j

105. Knoll W, Kasry A, Liu J, et al. Surface Plasmon Fluorescence Techniques for Bioaffinity Studies. In: Schasfoort RBM, Tudos AJ, eds. *Handbook of Surface Plasmon Resonance*. Cambridge, United Kingdom: Royal Society Of Chemistry; 2008:275-312. doi:10.1039/9781847558220-00275

106. Kooyman RPH. Physics of Surface Plasmon Resonance. In: Schasfoort RBM, Tudos AJ, eds. *Handbook of Surface Plasmon Resonance*. Cambridge, United Kingdom: Royal Society Of Chemistry; 2008:15-34. doi:10.1039/9780854042678-00015

107. Dahlin AB, Wittenberg NJ, Höök F, Oh S-H. Promises and Challenges of Nanoplasmonic Devices for Refractometric Biosensing. *J Invest Dermatol*. 2013;2(10):83-101. doi:10.1038/jid.2014.371

108. Colas F, Barchiesi D, Kessentini S, Toury T, Chapelle MLD La. Comparison of adhesion layers of gold on silicate glasses for SERS detection. *J Opt (United Kingdom)*. 2015;17(11):114010. doi:10.1088/2040-8978/17/11/114010

109. Gedig ET. Surface Chemistry in SPR Technology. In: Schasfoort RBM, Tudos AJ, eds. *Handbook of Surface Plasmon Resonance*. Cambridge, United Kingdom: Royal Society Of Chemistry; 2008:173-220. doi:10.1039/9780854042678-00173

110. Asal M, Özen Ö, Şahinler M, Baysal HT, Polatoğlu İ. An overview of biomolecules , immobilization methods and support materials of biosensors. *Sens Rev*. 2018;39(3):377-386. doi:10.1108/SR-04-2018-0084

111. Dostálek J, Ladd J, Jiang S, Homola J. SPR Biosensors for Detection of Biological and Chemical Analytes. In: Homola J, ed. *Surface Plasmon Resonance Based Sensors*. Heidelberg: Springer-Verlag; 2006:177-190. doi:10.1007/5346_019

112. Knoll W. Self-assembled microstructures at interfaces. *Curr Opin Colloid Interface Sci*. 1996;1(1):137-143. doi:10.1016/S1359-0294(96)80054-9

113. Parikh AN, Allara DL. Self-Assembled Monolayers: A Versatile Tool for Biofunctionalization of Surfaces. In: Knoll W, ed. *Handbook of Biofunctional Surfaces*. 1st ed. New York: Taylor & Francis Group, LLC; 2012:1-29. doi:10.1201/b14900

114. Li B, Ye Q. Antifouling Surfaces of Self-assembled Thin Layer. In: Zhou F, ed. *Antifouling Surfaces and Materials*. Berlin,Heidelberg: Springer-Verlag; 2015:31-54. doi:10.1007/978-3-662-45204-2_2

115. Knoll W, Liley M, Piscevic D, Spinke J, Tarlov MJ. Supramolecular Architectures for the functionalization of solid surfaces. *Adv Biophys*. 1997;34:231-251.

116. Nelson KE, Gamble L, Jung LS, et al. Surface characterization of mixed self-assembled monolayers designed for streptavidin immobilization. *Langmuir*. 2001;17(9):2807-2816. doi:10.1021/la001111e

117. Ayres N. Polymer brushes: Applications in biomaterials and nanotechnology. *Polym Chem*. 2010;1(6):769-777. doi:10.1039/b9py00246d

118. Zhao B, Brittain WJ. Polymer brushes: Surface-immobilized macromolecules. *Prog Polym Sci*. 2000;25(5):677-710. doi:10.1016/S0079-6700(00)00012-5

119. Peng S, Bhushan B. Smart polymer brushes and their emerging applications. *RSC Adv*. 2012;2(23):8557-8578. doi:10.1039/c2ra20451g

120. Biacore. Biacore Sensor Surface Handbook. 2003. http://www.biophysics.bioc.cam.ac.uk/wp-

content/uploads/2011/02/SensorSurface_Handbook.pdf.

121. Ducker R, Garcia A, Zhang J, Chen T, Zauscher S. Polymeric and biomacromolecular brush nanostructures: Progress in synthesis, patterning and characterization. *Soft Matter*. 2008;4(9):1774-1786. doi:10.1039/b804861b

122. Heise C, Bier FF. Immobilization of DNA on microarrays. In: *Immobilisation of DNA on Chips II. Topics in Current Chemistry*. Vol 261. Berlin, Heidelberg: Springer; 2005:1-25. doi:10.1007/128_007

123. Teraoka I. *Polymer Solutions: An Introduction to Physical Properties*. New York: John Wiley & Sons, Inc.; 2002. doi:10.1002/0471224510

124. de Gennes PG. Conformations of Polymers Attached to an Interface. *Macromolecules*. 1980;13(5):1069-1075. doi:10.1021/ma60077a009

125. Kim M, Schmitt SK, Choi JW, Krutty JD, Gopalan P. From self-assembled monolayers to coatings: Advances in the synthesis and nanobio applications of polymer brushes. *Polymers (Basel)*. 2015;7(7):1346-1378. doi:10.3390/polym7071346

126. Wattendorf U, Merkle HP. PEGylation as a Tool for the Biomedical Engineering of. *J Pharm Sci*. 2008;97(11):4655-4669. doi:10.1002/jps.21350

127. Baryeh K, Takalkar S, Lund M, Liu G. Introduction to medical biosensors for point of care applications. In: Narayan RJ, ed. *Medical Biosensors for Point of Care (POC) Applications*. Elsevier Ltd; 2017:3-25. doi:10.1016/B978-0-08-100072-4.00001-0

128. Liu J, Zehui C, Lu Y. Functional Nucleic Acid Sensors. *Chem Rev*. 2012;109(5):1948-1998. doi:10.1021/cr030183i

129. Liu Y, Yu J. Oriented immobilization of proteins on solid supports for use in biosensors and biochips: a review. *Microchim Acta*. 2016;183(1):1-19. doi:10.1007/s00604-015-1623-4

130. Hermanson GT. The Reactions of Bioconjugation. In: *Bioconjugate Techniques*. 3rd ed. 2013 Elsevier Inc.; 2013:127-258. doi:doi.org/10.1016/C2009-0-64240-9

131. Thermo Scientific. Crosslinking Technical Handbook. *Easy Mol Bond Crosslink Technol*. 2012:1-53. https://tools.thermofisher.com/content/sfs/brochures/1602163-Crosslinking-Reagents-Handbook.pdf.

132. Wilchek M, Bayer EA. Introduction to avidin-biotin technology. In: *Methods in Enzymology*. Vol 184. ; 1990:5-13. doi:10.1016/0076-6879(90)84256-G

133. Thermo Scientific. Avidin-Biotin Technical Handbook. 2009:1-51. http://assets.thermofisher.com/TFS-Assets/LSG/brochures/1601675-Avidin-Biotin-Handbook.pdf.

134. Jain A, Cheng K. The Principles and Applications of Avidin-Based Nanoparticles in Drug Delivery and Diagnosis. *J Control Release*. 2017;245(3):27-40. doi:110.1016/j.jconrel.2016.11.016

135. Su X, Wu YJ, Robelek R, Knoll W. Surface plasmon resonance spectroscopy and quartz crystal microbalance study of streptavidin film structure effects on biotinylated DNA assembly and target DNA hybridization. *Langmuir*. 2005;21(1):348-353. doi:10.1021/la047997u

136. Bergström G, Mandenius CF. Orientation and capturing of antibody affinity ligands: Applications to surface plasmon resonance biochips. *Sensors Actuators, B Chem*. 2011;158(1):265-270. doi:10.1016/j.snb.2011.06.017

137. Roy I, Gupta MN. Bioaffinity Immobilization. In: Guisan JM, ed. *Methods in Biotechnology: Immobilization of Enzymes and Cells*. 2nd ed. Totowa: Human Press Inc.; 2006:107-116. doi:10.1007/978-1-59745-053-9_10

138. Zhao W, Ali MM, Brook MA, Li Y. Rolling circle amplification: Applications in nanotechnology and biodetection with functional nucleic acids. *Angew Chemie - Int Ed*. 2008;47(34):6330-6337. doi:10.1002/anie.200705982

139. Lizardi PM, Huang X, Zhu Z, Bray-Ward P, Thomas DC, Ward DC. Mutation detection and single-molecule counting using isothermal rolling-circle amplification. *Nat Genet*. 1998;19(3):225-232. doi:10.1038/898

140. Clausson CM, Arngården L, Ishaq O, et al. Compaction of rolling circle amplification products increases signal integrity and signal-to-noise ratio. *Sci Rep*. 2015;5(June):1-10. doi:10.1038/srep12317

141. Jarvius J, Melin J, Göransson J, et al. Digital quantification using amplified single-molecule detection. *Nat Methods*. 2006;3(9):725-727. doi:10.1038/nmeth916

142. Xiang Y, Deng K, Xia H, et al. Isothermal detection of multiple point mutations by a surface plasmon resonance biosensor with Au nanoparticles enhanced surface-anchored rolling circle amplification. *Biosens Bioelectron*. 2013;49:442-449. doi:10.1016/j.bios.2013.04.044

143. Hafner GJ, Yang IC, Woiter LC, Stafford MR, Giffard PM. Isothermal amplification and multimerization of dna by Bst DNA polymerase. *Biotechniques*. 2001;30(4):852-867. doi:10.2144/01304rr03

144. Xiang Y, Zhu X, Huang Q, Zheng J, Fu W. Real-time monitoring of mycobacterium genomic DNA with target-primed rolling circle amplification by a Au nanoparticle-embedded SPR biosensor. *Biosens Bioelectron*. 2015;66:512-519. doi:10.1016/j.bios.2014.11.021

145. Shi D, Huang J, Chuai Z, et al. Isothermal and rapid detection of pathogenic microorganisms using a nano-rolling circle amplification-surface plasmon resonance biosensor. *Biosens Bioelectron*. 2014;62:280-287. doi:10.1016/j.bios.2014.06.066

146. He P, Liu L, Qiao W, Zhang S. Ultrasensitive detection of thrombin using surface plasmon resonance and quartz crystal microbalance sensors by aptamer-based rolling circle amplification and nanoparticle signal enhancement. *Chem Commun*. 2014;50(12):1481-1484. doi:10.1039/c3cc48223e

147. Huang YY, Hsu HY, Huang CJC. A protein detection technique by using surface plasmon resonance (SPR) with rolling circle amplification (RCA) and nanogold-modified tags. *Biosens Bioelectron*. 2007;22(6):980-985. doi:10.1016/j.bios.2006.04.017

148. SKM_C36819061317010.pdf.

149. Barbee KD, Chandrangsu M, Huang X. Fabrication of DNA Polymer Brush Arrays by Destructive Micropatterning and Rolling-Circle Amplification. *Macromol Biosci*. 2011;11(5):607-617. doi:10.1002/mabi.201000373

150. Heidcamp W. Cell biology laboratory manual. Density and refractive indexes of sucrose. http://www.chem.ucla.edu/dept/Faculty/merchant/pdf/sucrose gradient refractive index.pdf. Published 2017.

151. Polyanskiy M. Refractive index data base. https://refractiveindex.info/. Accessed November 1, 2020.

152. Larsson C, Rodahl M, Höök F. Characterization of DNA immobilization and subsequent hybridization on a 2D arrangement of streptavidin on a biotin-modified lipid bilayer supported on SiO2. *Anal Chem*. 2003;75(19):5080-5087. doi:10.1021/ac034269n

153. Peterson AW, Wolf LK, Georgiadis RM. Hybridization of mismatched or partially matched DNA at surfaces. *J Am Chem Soc*. 2002;124(49):14601-14607. doi:10.1021/ja0279996

154. Barišić I, Schoenthaler S, Ke R, Nilsson M, Noehammer C, Wiesinger-Mayr H. Multiplex detection of antibiotic resistance genes using padlock probes. *Diagn Microbiol Infect Dis*. 2013;77(2):118-125. doi:10.1016/j.diagmicrobio.2013.06.013

155. Knoll W, Zizlsperger M, Liebermann T, et al. Streptavidin arrays as supramolecular architectures in surface-plasmon optical sensor formats. *Colloids Surfaces A Physicochem Eng Asp*. 2000;161(1):115-137. doi:10.1016/S0927-7757(99)00331-3

156. Rosano C, Arosio P, Bolognesi M. The X-ray three-dimensional structure of avidin. *Biomol Eng*. 1999;16(1-4):5-12. doi:10.1016/S1050-3862(99)00047-9

157. Tsortos A, Papadakis G, Mitsakakis K, Melzak KA, Gizeli E. Quantitative determination of size and shape of surface-bound DNA using an acoustic wave sensor. *Biophys J*. 2008;94(7):2706-2715. doi:10.1529/biophysj.107.119271

158. Thibault T, Degrouard J, Baril P, Pichon C, Midoux P, Malinge JM. Production of DNA minicircles

less than 250 base pairs through a novel concentrated DNA circularization assay enabling minicircle design with NF-κB inhibition activity. *Nucleic Acids Res*. 2017;45(5):e26. doi:10.1093/nar/gkw1034

159. Gil PS, Lacks DJ, Parisse P, Casalis L, Nkoua Ngavouka MD. Single-stranded DNA oligomer brush structure is dominated by intramolecular interactions mediated by the ion environment. *Soft Matter*. 2018;14(47):9675-9680. doi:10.1039/c8sm01743c
160. Rao AN, Grainger DW. Biophysical properties of nucleic acids at surfaces relevant to microarray performance. *Biomater Sci*. 2014;2(4):436-471. doi:10.1039/c3bm60181a
161. Nkoua Ngavouka MD, Bosco A, Casalis L, Parisse P. Determination of average internucleotide distance in variable density ssDNA nanobrushes in the presence of different cations species. *Macromolecules*. 2014;47(24):8748-8753. doi:10.1021/ma501712a
162. Castelino K, Kannan B, Majumdar A. Characterization of grafting density and binding efficiency of DNA and proteins on gold surfaces. *Langmuir*. 2005;21(5):1956-1961. doi:10.1021/la047943k
163. Herne TM, Tarlov MJ. Characterization of DNA probes immobilized on gold surfaces. *J Am Chem Soc*. 1997;119(38):8916-8920. doi:10.1021/ja9719586
164. Peterson AW. The effect of surface probe density on DNA hybridization. *Nucleic Acids Res*. 2001;29(24):5163-5168. doi:10.1093/nar/29.24.5163
165. Gong P, Levicky R. DNA surface hybridization regimes. *Proc Natl Acad Sci*. 2008;105(14):5301-5306. doi:10.1073/pnas.0709416105
166. Petrovykh DY, Kimura-Suda H, Whitman LJ, Tarlov MJ. Quantitative analysis and characterization of DNA immobilized on gold. *J Am Chem Soc*. 2003;125(17):5219-5226. doi:10.1021/ja029450c
167. Montgomery JL, Rejali N, Wittwer CT. Stopped-flow DNA polymerase assay by continuous monitoring of dNTP incorporation by fluorescence. *Anal Biochem*. 2013;441(2):133-139. doi:10.1016/j.ab.2013.07.008
168. Bracha D, Karzbrun E, Shemer G, Pincus PA, Bar-Ziv RH. Entropy-driven collective interactions in DNA brushes on a biochip. *Proc Natl Acad Sci U S A*. 2013;110(12):4534-4538. doi:10.1073/pnas.1220076110
169. Lehner R, Koota J, Maret G, Gisler T. Segment distributions of end-tethered polymers in a good solvent. *Phys Rev Lett*. 2006;96(10):1-4. doi:10.1103/PhysRevLett.96.107801

9. List of Figures

10. List of Tables